Weak Gravitational Lensing

Martin Kilbinger

CEA Saclay, Irfu/SAp - AIM, CosmoStat; IAP

DarkMod IPhT, Saclay/Orsay
September/October 2017

martin.kilbinger@cea.fr
www.cosmostat.org/kilbinger

Slides: http://www.cosmostat.org/events/darkmod-2017

@energie_sombre #DarkMod

Overview

Day 1: Principles of gravitational lensing

- Brief history of gravitational lensing
- Light deflection in an inhomogeneous Universe
- Convergence, shear, and ellipticity
- Projected power spectrum
- Real-space shear correlations

Day 2: Measurement of weak lensing

- Galaxy shape measurement
- PSF correction
- Photometric redshifts
- Estimating shear statistics

Day 3: Surveys and cosmology

- Cosmological modelling
- Results from past and ongoing surveys (CFHTLenS, KiDS, DES)
- Euclid

Day 3+: Extra stuff

- Cluster lensing; nature of DM; tests of GR

Books, Reviews and Lecture Notes

- Bartelmann & Schneider 2001, review Weak gravitational lensing, Phys. Rep., 340, 297 arXiv:9912508
- Kochanek, Schneider & Wambsganss 2004, book (Saas Fee) Gravitational lensing: Strong, weak & micro. Download Part I (Introduction) and Part III (Weak lensing) from my homepage `http://www.cosmostat.org/kilbinger`.
- Kilbinger 2015, review Cosmology from cosmic shear observations Reports on Progress in Physics, 78, 086901, arXiv:1411.0155
- Bartelmann & Maturi 2017, review Weak gravitational lensing, Scholarpedia 12(1):32440, arXiv:1612.06535
- Henk Hoekstra 2013, lecture notes (Varenna) arXiv:1312.5981
- Sarah Bridle 2014, lecture videos (Saas Fee) `http://archiveweb.epfl.ch/saasfee2014.epfl.ch/page-110036-en.html`
- Alan Heavens, 2015, lecture notes (Rio de Janeiro) `www.on.br/cce/2015/br/arq/Heavens_Lecture_4.pdf`

Science with gravitational lensing

Let's start with a brief summary of outstanding results from gravitational lensing (micro, strong, weak).

Science with gravitational lensing

Outstanding results

Dark matter is not in form of massive compact objects (MACHOs).
Microlensing rules out objects between 10^{-7} and few 10 $M_\odot$.
[Larger masses possible, PBH, LIGO GW candidates?]

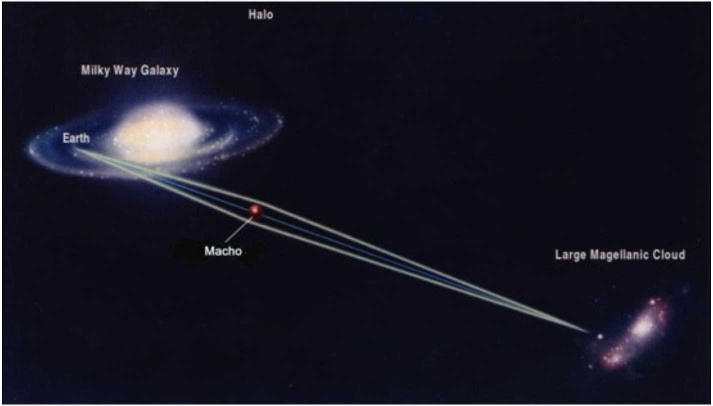

[Takahiro Sumi, Nagoya University]

Science with gravitational lensing

Outstanding results

Detection of Earth-like exoplanets with microlensing.
Masses and distances to host star similar to Earth.

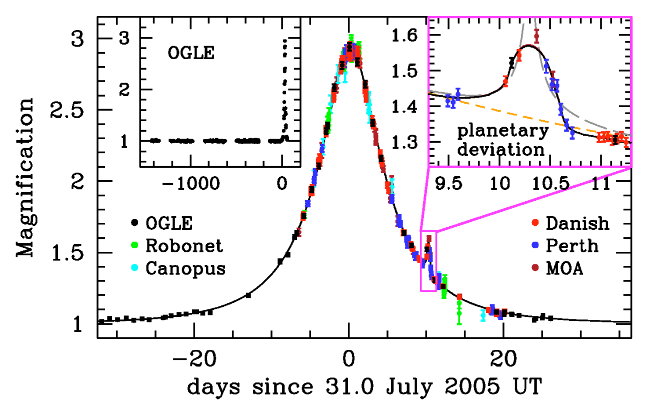

(?)

Science with gravitational lensing

Outstanding results

Structure of QSO inner emission regions.
Microlensing by stars in lens galaxies.

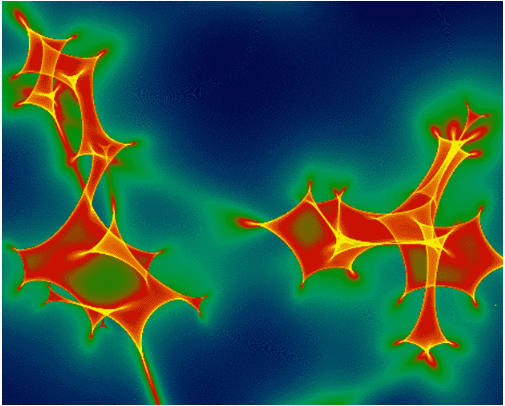

[J. Wambsganss]

Science with gravitational lensing

Outstanding results

Observation of very high ($z \geq 7$) galaxies.
Galaxy clusters as "natural telescopes".

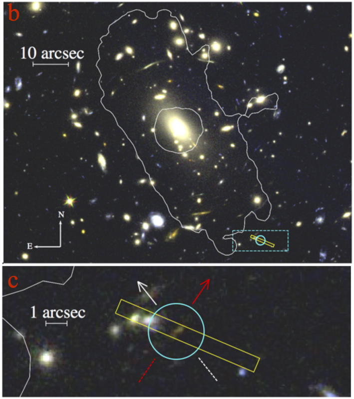

(?)

Science with gravitational lensing

Outstanding results

Galaxy clusters are dominated by dark matter.
Bullet cluster and others: bulk of mass is collisionless.

(Clowe et al. 2006)

Science with gravitational lensing

Outstanding results

Dark matter profiles in outskirts of galaxies.

Measuring halo mass to very large galactic scales.

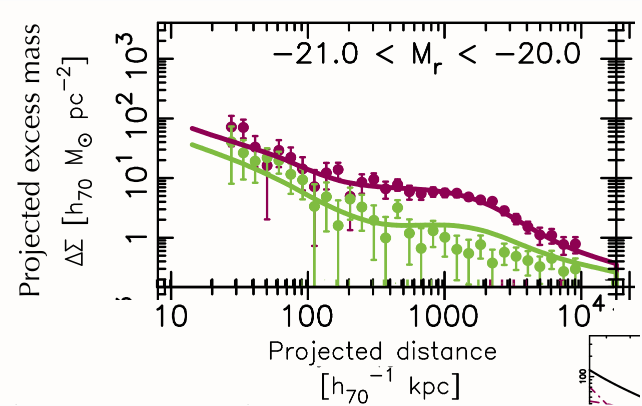

(Velander et al. 2014)

Science with gravitational lensing

Outstanding results

Hints of inconsistency of our cosmological model at low and high z?
Planck and WL in tension? Also WL cluster masses for Planck SZ clusters;
H_0 from cepheids + SL.

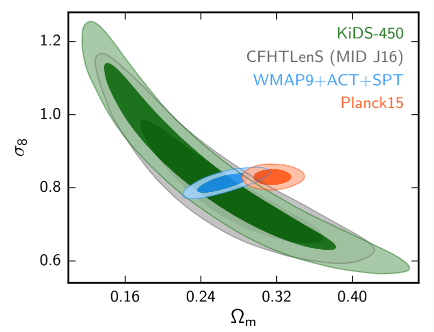

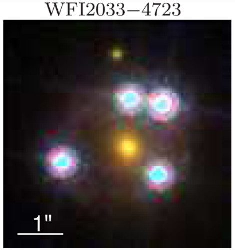

(Hildebrandt et al. 2017) (?)

Science with gravitational lensing

Outstanding results

General relativity holds on cosmological scales.
Joint WL and galaxy clustering cosmology-independent GR test.

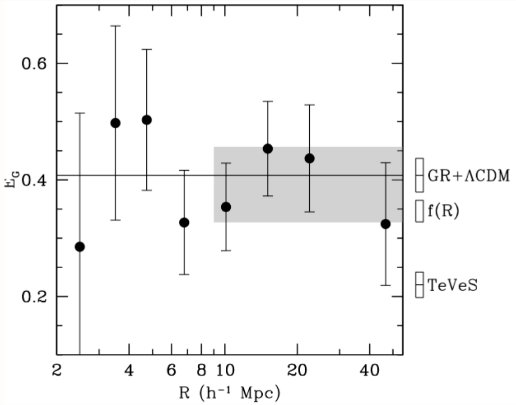

(Reyes et al. 2010)

Science with gravitational lensing

Outstanding results

Dark matter is not in form of massive compact objects (MACHOs).
Detection of Earth-mass exoplanets.
Structure of QSO inner emission regions.
Dark matter profiles in outskirts of galaxies.
Galaxy clusters are dominated by dark matter.
Observation of very-high ($z \geq 7$) galaxies.
Hints of inconsistency of our cosmological model at low and high z?
General relativity holds on cosmological scales.

Most important properties of gravitational lensing

Lensing probes total matter, baryonic + dark.
Independent of dynamical state of matter.
Independent of nature of matter.

Brief history of gravitational lensing

- Before Einstein: Masses deflect photons, treated as point masses.
- 1915 Einstein's GR predicted deflection of stars by sun, deflection larger by 2 compared to classical value. Confirmed 1919 by Eddington and others during solar eclipse.

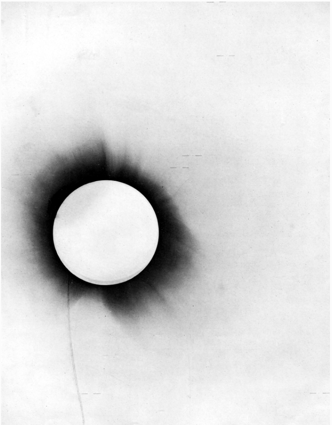

Photograph taken by Eddington of solar corona, and stars marked with bars.

Lensing on cosmological scales

- 1937 Zwicky posits galaxy clusters as lenses.
- 1979 Walsh et al. detect first double image of a lenses quasar.

Fritz Zwicky; Abell 2151 (Hercules galaxy cluster) ©Tony Hallas/APoD.

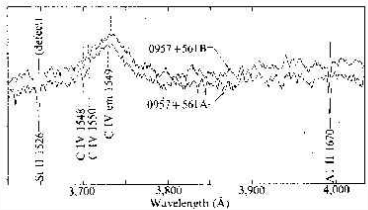

(Walsh et al. 1979)

- 1987 Soucail et al. strongly distorted “arcs” of background galaxies behind galaxy cluster, using CCDs.

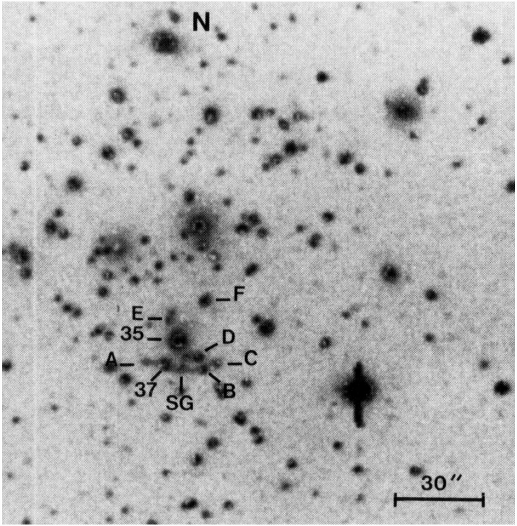

exclude that it is an off-chance superimposition of faint cluster galaxies even if a diffuse component seems quite clear from the R CCD field. A gravitational lens effect on a background quasar is a possibility owing to the curvature of the structure but in fact it is too small (Hammer 86) and no blue object opposite the central galaxy has been detected. It is more likely that we are dealing with a star formation region located in the very rich core where

- Tyson et al. (1990), tangential alignment around clusters.

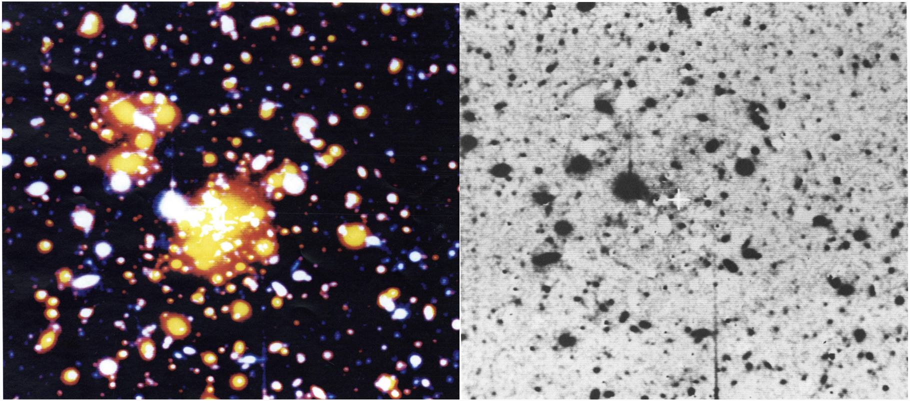

Abell 1689
Cluster outskirts: Weak gravitational lensing.

- 2000 cosmic shear: weak lensing in blind fields, by 4 groups (Edinburgh, Hawai'i, Paris, Bell Labs/US).
  Some 10,000 galaxies on few square degree on the sky area.

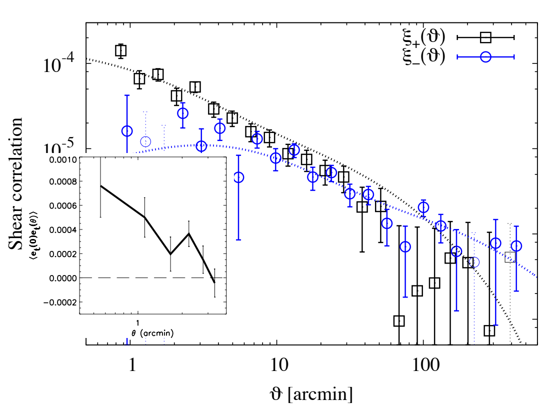

Shear (ellipticity) correlation of galaxies as fct. of angular separation (Van Waerbeke et al. 2000, Kilbinger et al. 2013).

- By 2016: Many dedicated surveys: DLS, CFHTLenS, DES, KiDS, HSC. Competitive constraints on cosmology.
  Factor 100 increase: Millions of galaxies over 100s of degree area. Many other improvements: Multi-band observations, photometric redshifts, image and N-body simulations, ...

- By 2025: LSST, WFIRST-AFTA, Euclid data will be available. Another factor of 100 increase: Hundred millions of galaxies, tens of thousands of degree area (most of the extragalactic sky).

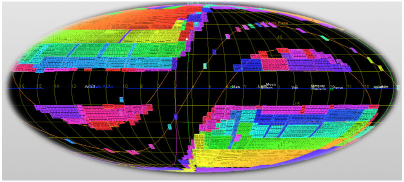

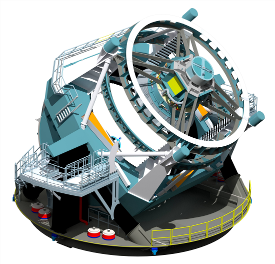

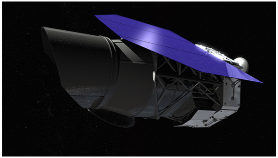

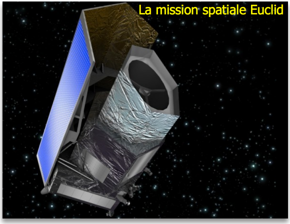

Types of lensing

source	lens	observation	name	science
star	star (≠sun)	time-varying magnification	micro-lensing	exoplanets, MACHOs, limb darkening
galaxy	galaxy, cluster	multiple images, arcs, Δt	strong lensing	galaxy *M/L*, properties inner cluster structure, dark-matter properties, *H0, QSO structure*
galaxies	galaxies, cluster LSS	distortions, magnification, σ(number density)	weak lensing	galaxy *M/L*, halos, cluster *M*, outer structure, cosmo parameters
CMB	LSS	distortions in T	CMB (weak) lensing	cosmo parameters

Types of lensing

source	lens	observation	name	science
star	star (≠sun)	time-varying magnification	micro-lensing	exoplanets, MACHOs, limb darkening
galaxy	galaxy, cluster	multiple images, arcs, Δt	strong lensing	galaxy *M/L*, properties inner cluster structure, dark-matter properties, *H0, QSO structure*
galaxies	galaxies, cluster **LSS**	**distortions**, magnification, σ(number density)	**weak lensing**	galaxy *M/L*, halos, cluster *M*, outer structure, **cosmo parameters**
CMB	LSS	distortions in T	CMB (weak) lensing	cosmo parameters

Cosmic shear, or weak cosmological lensing

Light of distant galaxies is deflected while travelling through inhomogeneous Universe. Information about mass distribution is imprinted on observed galaxy images.

- Continuous deflection: sensitive to projected 2D mass distribution.
- Differential deflection: magnification, distortions of images.
- Small distortions, few percent change of images: need statistical measurement.
- Coherent distortions: measure correlations, scales few Mpc to few 100 Mpc.

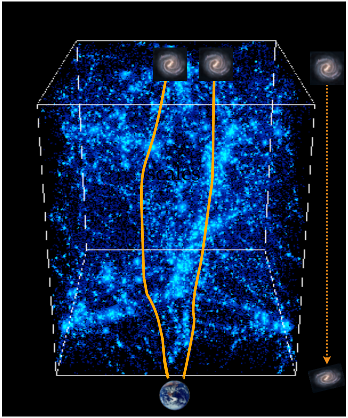

Measuring cosmic shear

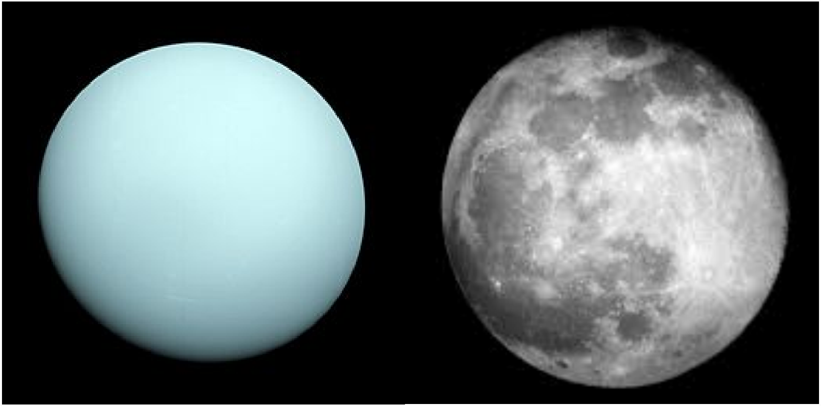

Typical shear of a few percent equivalent to difference in ellipticity between Uranus and the Moon.

Example: Euclid Visible imager (VIS)

This will be easy with Euclid. Right?

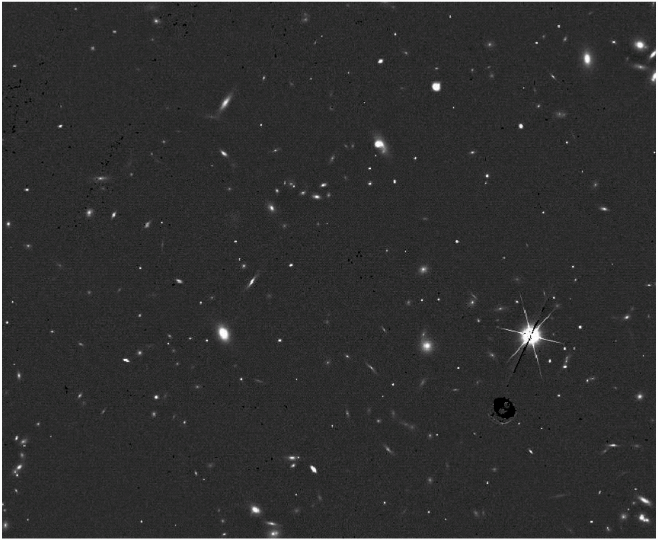

Simulation: Euclid VIS team, Henry McCracken (IAP).

Example: Euclid Visible imager (VIS)

This will be easy with Euclid. Riiiiight…

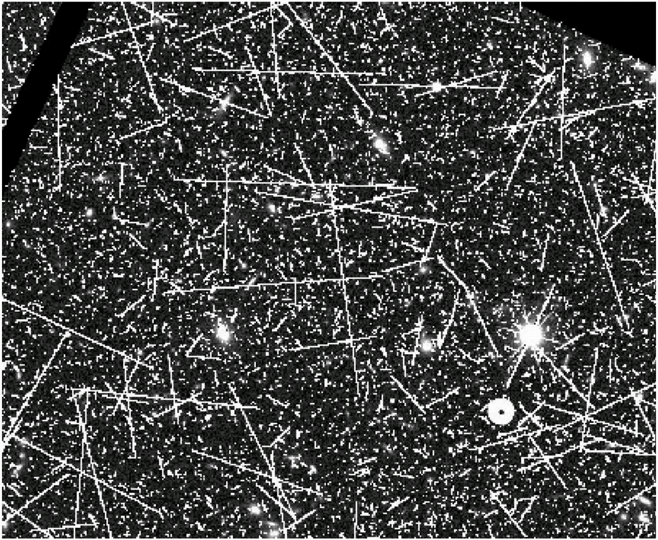

Simulation: Euclid VIS team, Henry McCracken (IAP).

Deflection angle

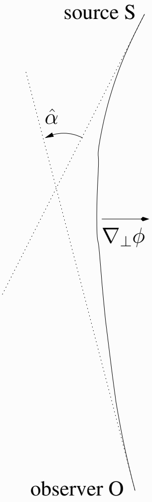

Perturbed Minkowski metric, weak-field ($\phi \ll c^2$)

$$\mathrm{d}s^2 = \left(1 + 2\phi/c^2\right) c^2 \mathrm{d}t^2 - \left(1 - 2\phi/c^2\right) \mathrm{d}\ell^2$$

One way to derive deflection angle: Fermat's principle:

$$\text{Light travel time} \qquad t = \frac{1}{c} \int_{\text{path}} \left(1 - 2\phi/c^2\right) \mathrm{d}\ell$$

is stationary, $\delta t = 0$. (Analogous to geometrical optics, potential as medium with refract. index $n = 1 - 2\phi/c^2$.) Integrate Euler-Lagrange equations along the light path to get

$$\text{deflection angle} \qquad \hat{\boldsymbol{\alpha}} = -\frac{2}{c^2} \int_{\text{S}}^{\text{O}} \boldsymbol{\nabla}_\perp \phi \, \mathrm{d}\ell$$

Special case: point mass

Deflection angle for a point mass M is

$$\hat{\boldsymbol{\alpha}} = \frac{4GM}{c^2 \xi} \frac{\boldsymbol{\xi}}{\xi} = \frac{2R_{\rm S}}{\xi} \frac{\boldsymbol{\xi}}{\xi}$$

($R_{\rm S}$ is the Schwarzschild radius.)

This is twice the value one would get in a classical, Newtonian calculation.

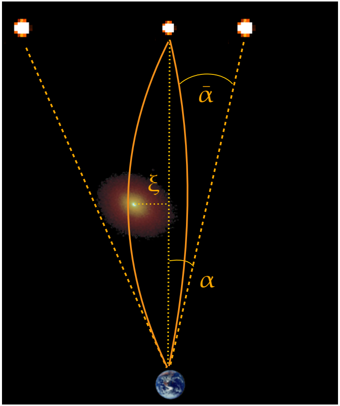

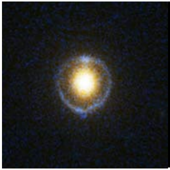

SDSS J1627-0053
$z_s = 0.5$, $z_l = 0.2$, $\alpha = 2.8''$ (5 kpc)

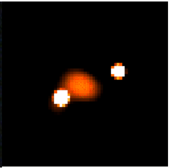

HE 1104-1825
$z_s = 2.3$, $z_l = 1.7$, $\alpha = 1.6''$ (14 kpc)

Exercise: Derive the deflection angle for a point mass. I

We can approximate the potential as

$$\phi = -\frac{GM}{R} = -\frac{c^2}{2}\frac{R_\mathrm{S}}{R},$$

where G is Newton's constant, M the mass of the object, R the distance, and R_S the Schwarzschild radius.

The distance R can be written as $R^2 = x^2 + y^2 + z^2$.
(Weak-field condition $\phi \ll c^2$ implies $R \gg R_\mathrm{S}$.
(Here z is not redshift, but radial (comoving) distance.)

We use the so-called Born approximation (from quantum mechanic scattering theory) to integrate along the unperturbed light ray, which is a straight line parallel to the z-axis with a constant $x^2 + y^2 = \xi^2$.

The impact parameter ξ is the distance of the light ray to the point mass.

Exercise: Derive the deflection angle for a point mass. II

The deflection angle is then

$$\hat{\boldsymbol{\alpha}} = -\frac{2}{c^2} \int_{-\infty}^{\infty} \boldsymbol{\nabla}_\perp \phi \, \mathrm{d}z.$$

The perpendicular gradient of the potential is

$$\boldsymbol{\nabla}_\perp \phi = \frac{c^2 R_\mathrm{S}}{2|R|^3} \begin{pmatrix} x \\ y \end{pmatrix} = \frac{c^2 R_\mathrm{S}}{2} \frac{\xi}{(\xi^2 + z^2)^{3/2}} \begin{pmatrix} \cos\varphi \\ \sin\varphi \end{pmatrix}.$$

The primitive for $(\xi^2 + z^2)^{-3/2}$ is $z\xi^{-2}(\xi^2 + z^2)^{-1/2}$. We use the symmetry of the integrand to integrate between 0 and ∞, and get for the absolute value of the deflection angle

$$\hat{\alpha} = 2R_\mathrm{S} \left[\frac{z}{\xi(\xi^2 + z^2)^{1/2}} \right]_0^\infty = \frac{2R_\mathrm{S}}{\xi} = \frac{4GM}{c^2 \xi}.$$

Generalisation I: mass distribution

Distribution of point masses $M_i(\boldsymbol{\xi}_i, z)$: total deflection angle is linear vectortial sum over individual deflections

$$\hat{\boldsymbol{\alpha}}(\boldsymbol{\xi}) = \sum_i \hat{\boldsymbol{\alpha}}(\boldsymbol{\xi} - \boldsymbol{\xi}_i) = \frac{4G}{c^2} \sum_i M_i(\boldsymbol{\xi}_i, z) \frac{\boldsymbol{\xi} - \boldsymbol{\xi}_i}{|\boldsymbol{\xi} - \boldsymbol{\xi}_i|}$$

With transition to continuous density

$$M_i(\boldsymbol{\xi}_i, z) \to \int \mathrm{d}^2\xi' \int \mathrm{d}z' \, \rho(\boldsymbol{\xi}', z')$$

and introduction of the 2D

$$\text{surface mass density} \quad \Sigma(\boldsymbol{\xi}') = \int \mathrm{d}z' \, \rho(\boldsymbol{\xi}', z')$$

we get

$$\hat{\boldsymbol{\alpha}}(\boldsymbol{\xi}) = \int \mathrm{d}^2\xi' \, \Sigma(\boldsymbol{\xi}') \frac{\boldsymbol{\xi} - \boldsymbol{\xi}'}{|\boldsymbol{\xi} - \boldsymbol{\xi}'|}$$

Thin-lens approximation

Generalisation II: Extended source I

Extended source: different light rays impact lens at different positions $\boldsymbol{\xi}$, their deflection angle $\boldsymbol{\alpha}(\boldsymbol{\xi})$ will be different: differential deflection $\rightarrow$ distortion, magnification of source image!

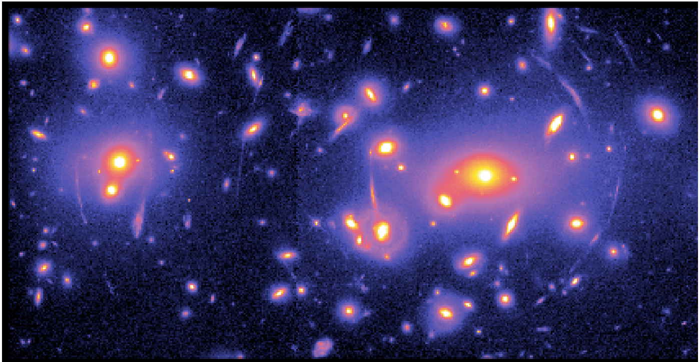

The cluster of galaxies Abell 2218

Propagation of light bundles I

Calculate deflection angle difference between different light bundles:

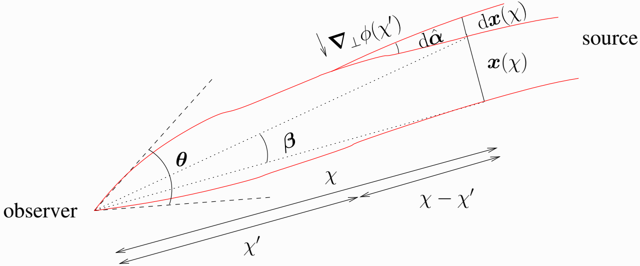

In homogeneous flat Universe, transverse distance $\boldsymbol{x}_0$ between two light rays as fct. of comoving distance χ

$$\boldsymbol{x}_0(\chi) = \chi \boldsymbol{\theta}.$$

This is modified by inhomogeneous matter = deflectors as follows.

Propagation of light bundles II

From deflector at comoving distance χ', infinitesimal deflection angle

$$\mathrm{d}\hat{\boldsymbol{\alpha}} = -\frac{2}{c^2}\,\boldsymbol{\nabla}_\perp \phi(\boldsymbol{x}, \chi')\mathrm{d}\chi'$$

This results in a change of transverse distance $\mathrm{d}x$ from vantage point of deflector (at χ')

$$\mathrm{d}\boldsymbol{x} = (\chi - \chi')\mathrm{d}\hat{\boldsymbol{\alpha}}$$

Total deflection: integrate over all deflectors along χ'. This would yield the difference between a perturbed and an unperturbed light ray. To account for perturbation of second light ray, subtract gradient of potential $\phi^{(0)}$ along second light ray.

$$\boldsymbol{x}(\chi) = \chi\boldsymbol{\theta} - \frac{2}{c^2}\int_0^\chi \mathrm{d}\chi'(\chi - \chi')\left[\boldsymbol{\nabla}_\perp \phi(\boldsymbol{x}(\chi'), \chi') - \boldsymbol{\nabla}_\perp \phi^{(0)}(\chi')\right].$$

Transform distances into angles seen from the observer: divide by χ. $\boldsymbol{x}/\chi$ is the angle $\boldsymbol{\beta}$ under which the unlensed source is seen. The integral/χ is the

Propagation of light bundles III

geometric difference between unlensed ($\boldsymbol{\beta}$) and apparent, lensed ($\boldsymbol{\theta}$), the deflection angle

$$\boldsymbol{\alpha} = \frac{2}{c^2} \int_0^\chi \mathrm{d}\chi' \frac{\chi - \chi'}{\chi} \left[\boldsymbol{\nabla}_\perp \Phi(\boldsymbol{x}(\chi'), \chi') - \boldsymbol{\nabla}_\perp \Phi^{(0)}(\chi') \right].$$

This results in the lens equation

$$\begin{aligned}\boldsymbol{\beta} &= \boldsymbol{\theta} - \boldsymbol{\alpha} \\ &= \boldsymbol{\theta} - \frac{2}{c^2} \int_0^\chi \mathrm{d}\chi' \frac{\chi - \chi'}{\chi} \left[\boldsymbol{\nabla}_\perp \Phi(\chi' \boldsymbol{\theta}, \chi'), \chi') - \boldsymbol{\nabla}_\perp \Phi^{(0)}(\chi') \right].\end{aligned}$$

This is a mapping from lens coordinates $\boldsymbol{\theta}$ to source coordinates $\boldsymbol{\beta}$.

(Q: why not the other way round?)

Linearized lensing quantities I

To 0^{th} order: approximate light path $\boldsymbol{x}$, on which potential gradient is evaluated in integral with unperturbed line $\chi\boldsymbol{\theta}$ (Born approximation):

$$\boldsymbol{\beta}(\boldsymbol{\theta}) = \boldsymbol{\theta} - \frac{2}{c^2} \int_0^\chi \mathrm{d}\chi' \frac{\chi - \chi'}{\chi} \left[\boldsymbol{\nabla}_\perp \Phi(\chi'\boldsymbol{\theta}, \chi'), \chi') - \boldsymbol{\nabla}_\perp \Phi^{(0)}(\chi') \right].$$

This neglects coupling between structures at different distances (*lens-lens coupling*): Distortion at some distance adds to undistorted image, neglecting distortion effect on already distorted image by all matter up to that distance.

Numerical simulations show that Born is accurate to sub-percent on most scales. This is pretty cool. Differences between perturbed and unberturbed light ray can be a few Mpc!

Next, drop the second term (does not depend on distance $\boldsymbol{x} = \chi\theta$, so gradient vanishes).

Linearized lensing quantities II

Now, we can move the gradient out of integral. That means, deflection angle is a gradient of a potential, the 2D lensing potential ψ. Writing derivatives with respect to angle $\boldsymbol{\theta}$, we get

$$\boldsymbol{\beta}(\boldsymbol{\theta}, \chi) = \boldsymbol{\theta} - \boldsymbol{\nabla}_{\boldsymbol{\theta}} \psi(\boldsymbol{\theta}, \chi)$$

with

$$\psi(\boldsymbol{\theta}, \chi) = \frac{2}{c^2} \int_0^\chi \mathrm{d}\chi' \, \frac{\chi - \chi'}{\chi \chi'} \, \phi(\chi' \boldsymbol{\theta}, \chi').$$

[Note: Above equations are valid for flat Universe. For general (curved) models, some comoving distances are replaced by comoving angular distances.]

Linearized lensing quantities III

Linearizing lens equation

We talked about differential deflection before. To first order, this involves the derivative of the deflection angle.

Or the lens mapping:

$$\frac{\partial \beta_i}{\partial \theta_j} \equiv A_{ij} = \delta_{ij} - \partial_i \partial_j \psi .$$

Jacobi (symmetric) matrix

$$A = \begin{pmatrix} 1-\kappa-\gamma_1 & -\gamma_2 \\ -\gamma_2 & 1-\kappa+\gamma_1 \end{pmatrix} .$$

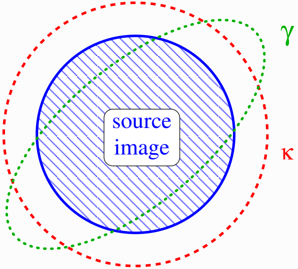

- convergence κ: isotropic magnification
- shear γ: anisotropic stretching

Convergence and shear are second derivatives of the 2D lensing potential.

Convergence and shear I

The effect of κ and γ follows from Liouville's theorem: Surface brightness is conserved (no photon gets lost).
Therefore the surface brightness I at the lensed position $\boldsymbol{\theta}$ is equal to the unlensed, source surface brightness $I^{\rm s}$ at the source position $\boldsymbol{\beta}$.

$$I(\boldsymbol{\theta}) = I^{\rm s}(\boldsymbol{\beta}(\boldsymbol{\theta})) \approx I^{\rm s}(\boldsymbol{\beta}(\boldsymbol{\theta}_0) + \mathcal{A}(\boldsymbol{\theta} - \boldsymbol{\theta}_0))$$

The second step is from Taylor expansion of lens equation around angle $\boldsymbol{\theta}_0$:

$$\boldsymbol{\beta}(\boldsymbol{\theta}) = \boldsymbol{\beta}(\boldsymbol{\theta}_0) + \frac{\partial \boldsymbol{\beta}}{\partial \boldsymbol{\theta}} (\boldsymbol{\theta} - \boldsymbol{\theta}_0) + \ldots$$

Example: circular isophotes

Effect can easily be seen for circular source isophotes,
e.g. $\theta_1 = R \cos t, \theta_2 = R \sin t$ (thus $\theta_1^2 + \theta_2^2 = R^2$).

Convergence

Applying the Jacobi matrix with zero shear (and setting $\boldsymbol{\beta}(\theta_0) = 0$), we find $\beta_1^2 + \beta_2^2 = R^2(1-\kappa)^2$. The radius R of these isophotes gets transformed at source position to $R(1-\kappa)$.

Convergence and shear II

Shear

To see an example for the shear stretching, set $\gamma_2 = 0$. We find $(\beta_1, \beta_2) = R([1-\kappa-\gamma_1]\cos t, [1-\kappa+\gamma_1]\sin t)$ and thus $(\beta_1/[1-\kappa-\gamma_1])^2 + (\beta_2/[1-\kappa+\gamma_1])^2 = R^2$, which is an ellipse with half axes $R/[1-\kappa-\gamma_1]$ and $R/[1-\kappa+\gamma_1]$.

So we see that shear transforms a circular image into an elliptical one.

Define complex shear

$$\gamma = \gamma_1 + \mathrm{i}\gamma_2 = |\gamma| \mathrm{e}^{2\mathrm{i}\varphi};$$

The relation between convergence, shear, and the axis ratio of elliptical isophotes is then

$$|\gamma| = |1-\kappa| \frac{1-b/a}{1+b/a}$$

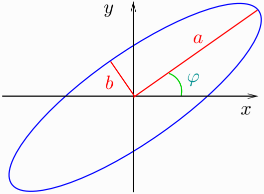

Convergence and shear III

Further consequence of lensing: magnification.
Liouville (surface brightness is conserved) + area changes ($\mathrm{d}\beta^2 \neq \mathrm{d}\theta^2$ in general) $\rightarrow$ flux changes.

$$\text{magnification} \quad \mu = \det A^{-1} = \left[(1-\kappa)^2 - \gamma^2\right]^{-1}.$$

Summary: Convergence and shear linearly encompass information about projected mass distribution (lensing potential ψ). They quantify how lensed images are magnified, enlarged, and stretched. These are the main observables in (weak) lensing.

Effects of lensing, $\partial^i \psi / \partial x^i$

i	symbol	name	spin	effect
0	Δt	time delay	0	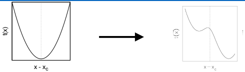
1	α	deflection	1	
2	κ	convergence	0	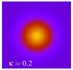
2	γ	shear	2	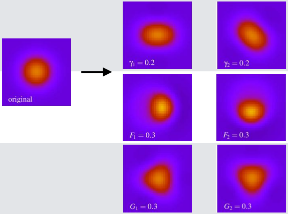
3	F	flextion	1	
3	G	flexion	3	

image credit Massimo

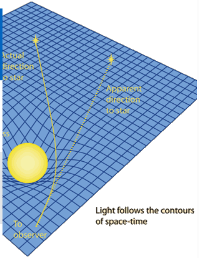

Basic equation of weak lensing

Weak lensing regime

$\kappa \ll 1, |\gamma| \ll 1.$

The observed ellipticity of a galaxy is the sum of the intrinsic ellipticity and the shear:

$$\boxed{\varepsilon^{\rm obs} \approx \varepsilon^{\rm s} + \gamma}$$

Random intrinsic orientation of galaxies

$$\langle \varepsilon^{\rm s} \rangle = 0 \quad \longrightarrow \quad \boxed{\langle \varepsilon \rangle = \gamma}$$

The observed ellipticity is an unbiased estimator of the shear. Very noisy though! $\sigma_\varepsilon = \langle |\varepsilon^{\rm s}|^2 \rangle^{1/2} \approx 0.4 \gg \gamma \sim 0.03$. Increase S/N and beat down noise by averaging over large number of galaxies.

Question: Why is the equivalent estimation of the convergence and/or magnification more difficult?

Ellipticity and local shear

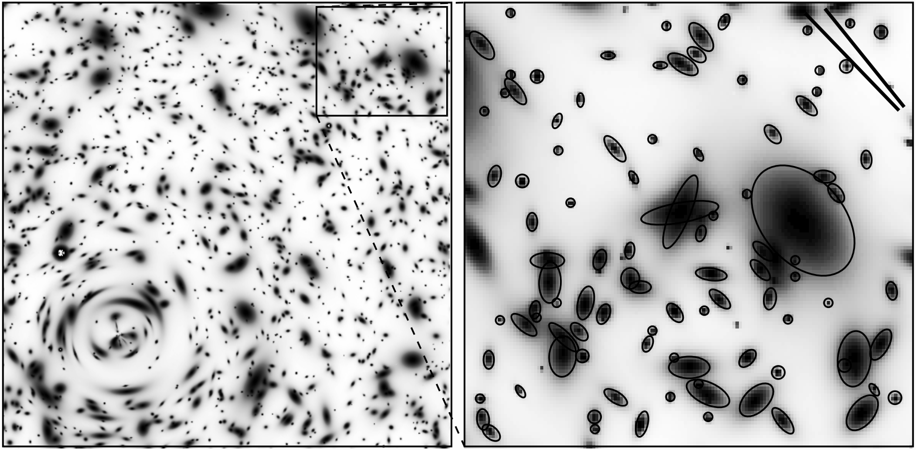

[from Y. Mellier]

Galaxy ellipticities are an estimator of the local shear.

Some weak-lensing galaxy surveys

Survey	Date	Area [deg^2]	$n_{\rm gal}$ [arcmin^{-2}]
CFHTLenS	2003-2007	170	14
DLS	2001-2006	25	20
COSMOS	2005	1.6	80
SDSS	2000-2012	11,000	2
KiDS	2011-	1,500	7-8
HSC	2015-	1,500	~~$\sim$ 20~~ 22
DES	2012-2018	5,000	3-6
CFIS	2017-2020	5,000	$\sim$ 6-7
LSST	2021-	15,000	30 - 40
Euclid	2021-2026	15,000	$\sim$ 30
WFIRST-AFTA	2024-	2,500	$\sim$ 50

Convergence and cosmic density contrast

Back to the lensing potential

- Since $\kappa = \frac{1}{2}\Delta\psi$:

$$\kappa(\boldsymbol{\theta}, \chi) = \frac{1}{c^2} \int_0^\chi \mathrm{d}\chi' \frac{(\chi - \chi')\chi'}{\chi} \Delta_{\boldsymbol{\theta}} \Phi(\chi' \boldsymbol{\theta}, \chi')$$

- Terms $\Delta_{\chi'\chi'}\Phi$ average out when integrating along line of sight, can be added to yield 3D Laplacian (error $\mathcal{O}(\Phi) \sim 10^{-5}$).
- Poisson equation

$$\Delta\Phi = \frac{3H_0^2\Omega_\mathrm{m}}{2a}\,\delta \qquad \left(\delta = \frac{\rho - \bar\rho}{\bar\rho}\right)$$

$$\to \kappa(\boldsymbol{\theta}, \chi) = \frac{3}{2}\Omega_\mathrm{m}\left(\frac{H_0}{c}\right)^2 \int_0^\chi \mathrm{d}\chi' \frac{(\chi - \chi')\chi'}{\chi a(\chi')}\,\delta\left(\chi'\boldsymbol{\theta}, \chi'\right).$$

Amplitude of the cosmic shear signal

Order-of magnitude estimate

$$\kappa(\boldsymbol{\theta}, \chi) = \frac{3}{2} \Omega_{\rm m} \left(\frac{H_0}{c} \right)^2 \int_0^\chi {\rm d}\chi' \, \frac{(\chi - \chi')\chi'}{\chi a(\chi')} \, \delta \left(\chi' \boldsymbol{\theta}, \chi' \right) .$$

for simple case: single lens at at redshift $z_{\rm L} = 0.4$ with comoving size $R/a(z_L)$, source at $z_{\rm S} = 0.8$.

$$\kappa \approx \frac{3}{2} \Omega_{\rm m} \left(\frac{H_0}{c} \right)^2 \frac{D_{\rm LS} D_{\rm L}}{D_{\rm S}} \frac{R}{a^2(z_{\rm L})} \frac{\delta\rho}{\rho}$$

Add signal from $N \approx D_{\rm S}/[R/a(z_{\rm L})]$ crossings, calculate rms:

$$\begin{aligned} \langle \kappa^2 \rangle^{1/2} & \approx \frac{3}{2} \Omega_{\rm m} \frac{D_{\rm LS} D_{\rm L}}{R_{\rm H}^2} \sqrt{\frac{R}{D_{\rm S}}} a^{-1.5}(z_{\rm L}) \left\langle \left(\frac{\delta\rho}{\rho} \right)^2 \right\rangle^{1/2} \\ & \approx \frac{3}{2} \, 0.3 \times 0.1 \quad \times \; 0.1 \quad \times 2 \qquad \quad \times 1 \qquad \approx 0.01 \end{aligned}$$

We are indeed in the weak-lensing regime.

Convergence with source redshift distribution

So far, we looked at the convergence for one single source redshift (distance χ). Now, we calculate κ for a realistic survey with a redshift distribution of source galaxies. We integrate over the pdf $p(\chi)\mathrm{d}\chi = p(z)\mathrm{d}z$, to get

$$\kappa(\boldsymbol{\theta}) = \int_0^{\chi_{\rm lim}} \mathrm{d}\chi \, p(\chi) \, \kappa(\boldsymbol{\theta}, \chi) = \int_0^{\chi_{\rm lim}} \mathrm{d}\chi \, G(\chi) \, \chi \, \delta\left(\chi\boldsymbol{\theta}, \chi\right)$$

with lens efficiency

$$G(\chi) = \frac{3}{2}\left(\frac{H_0}{c}\right)^2 \frac{\Omega_{\rm m}}{a(\chi)} \int_\chi^{\chi_{\rm lim}} \mathrm{d}\chi' \, p(\chi') \frac{\chi' - \chi}{\chi'}.$$

The convergence is a projection of the matter-density contrast, weighted by the source galaxy distribution and angular distances.

Parametrization of redshift distribution, e.g.

$$p(z) \propto \left(\frac{z}{z_0}\right)^{\alpha} \exp\left[-\left(\frac{z}{z_0}\right)^{\beta}\right]$$

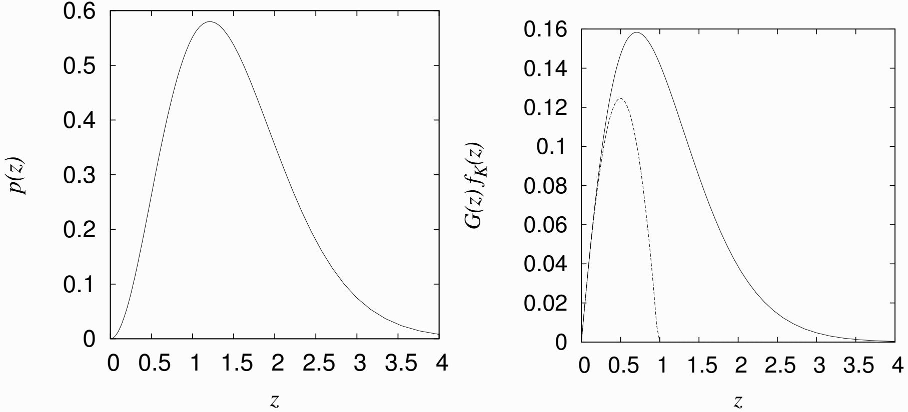

$\alpha = 2, \beta = 1.5, z_0 = 1$
(dashed line: all sources at redshift 1)

Max. lensing signal from halfway distance between us and lensing galaxies.

The relation between κ and γ

Convergence and shear are second derivatives of lensing potential $\rightarrow$ they are related.
One can derive κ from γ (except constant *mass sheet* κ_0).
E.g. get projected mass reconstruction of clusters from ellipticity observations.

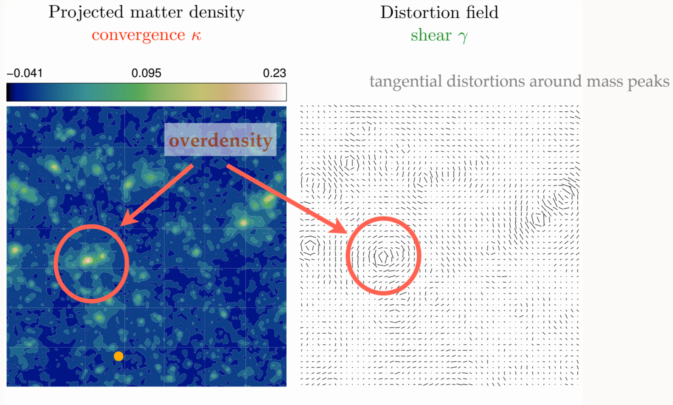

Source galaxies at $z = 1$, ray-tracing simulations by T. Hamana

The relation between κ and γ

Convergence and shear are second derivatives of lensing potential $\rightarrow$ they are related.
Fluctuations (variance σ^2) in κ and γ are the same!
E.g. get variance/power spectrum of projected δ from ellipticity correlations.

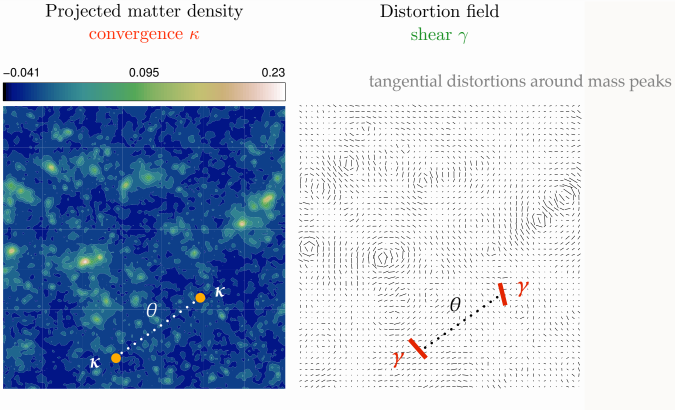

Source galaxies at $z = 1$, ray-tracing simulations by T. Hamana

The convergence power spectrum

- Variance of convergence $\langle \kappa(\boldsymbol{\vartheta} + \boldsymbol{\theta})\kappa(\boldsymbol{\vartheta})\rangle = \langle \kappa\kappa\rangle(\theta)$ depends on variance of the density contrast $\langle \delta\delta\rangle$
- In Fourier space:

$$\left\langle \hat\kappa(\boldsymbol{\ell})\hat\kappa^*(\boldsymbol{\ell}')\right\rangle = (2\pi)^2\delta_{\rm D}(\boldsymbol{\ell} - \boldsymbol{\ell}')P_\kappa(\ell)$$
$$\left\langle \hat\delta(\boldsymbol{k})\hat\delta^*(\boldsymbol{k}')\right\rangle = (2\pi)^3\delta_{\rm D}(\boldsymbol{k} - \boldsymbol{k}')P_\delta(k)$$

- Limber's equation

$$P_\kappa(\ell) = \int {\rm d}\chi\, G^2(\chi)P_\delta\left(k = \frac{\ell}{\chi}\right)$$

using small-angle approximation, $P_\delta(k) \approx P_\delta(k_\perp)$, contribution only from Fourier modes $\perp$ to line of sight. Also assumes that power spectrum varies slowly.

Dependence on cosmology

initial conditions,
growth of structure

$$P_\kappa(\ell) = \int \mathrm{d}\chi \, G^2(\chi) P_\delta\left(k = \frac{\ell}{\chi}\right)$$

$$G(\chi) = \frac{3}{2}\left(\frac{H_0}{c}\right)^2 \frac{\Omega_\mathrm{m}}{a(\chi)} \int_\chi^{\chi_\mathrm{lim}} \mathrm{d}\chi' \, p(\chi') \frac{\chi' - \chi}{\chi'}$$

matter density

redshift distribution
of source galaxies

geometry

Example

A simple toy model: single lens plane at redshift z_0, $P_\delta(k) \propto \sigma_8^2 k^n$, CDM, no Λ, linear growth:

$$\langle \kappa^2(\theta) \rangle^{1/2} = \langle \gamma^2(\theta) \rangle^{1/2} \approx 0.01\, \sigma_8\, \Omega_{\rm m}^{0.8} \left(\frac{\theta}{1 \rm deg} \right)^{-(n+2)/2} z_0^{0.75}$$

This simple example illustrates three important facts about measuring cosmology from weak lensing:

1. The signal is very small ($\sim$ percent)
2. Parameters are degenerate
3. The signal depends on source galaxy redshift

Lensing 'tomography' (2 1/2 D lensing)

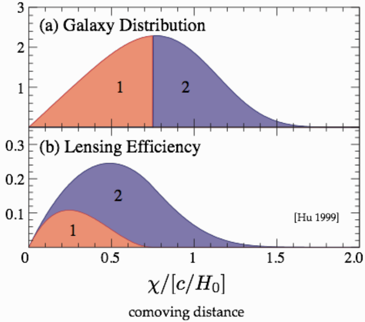

- Bin galaxies in redshift.
- Lensing efficiency different for different bins (even though the probed redshift range is overlapping): measure z-depending expansion and growth history.
- Necessary to measure dark energy, modified gravity.

$$P_\kappa(\ell) = \int_0^{\chi_{\rm lim}} \mathrm{d}\chi\, G^2(\chi) P_\delta\left(k = \frac{\ell}{\chi}\right) \rightarrow$$

$$P_\kappa^{ij}(\ell) = \int_0^{\chi_{\rm lim}} \mathrm{d}\chi\, G_i(\chi) G_j(\chi) P_\delta\left(k = \frac{\ell}{\chi}\right)$$

$$G_i(\chi) = \frac{3}{2}\left(\frac{H_0}{c}\right)^2 \frac{\Omega_{\rm m}}{a(\chi)} \int_\chi^{\chi_{\rm lim}} \mathrm{d}\chi'\, p_i(\chi') \frac{\chi' - \chi}{\chi'}.$$

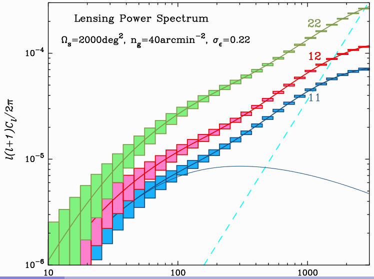

Convergence power spectrum for two different redshift bins $(0 = [0.5; 0.7], 1 = [0.9; 1.1])$.

Unlike CMB C_ℓ's, features in matter power spectrum are washed out by projection and non-linear evolution.

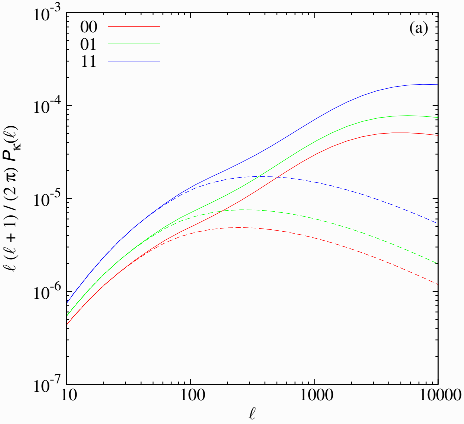

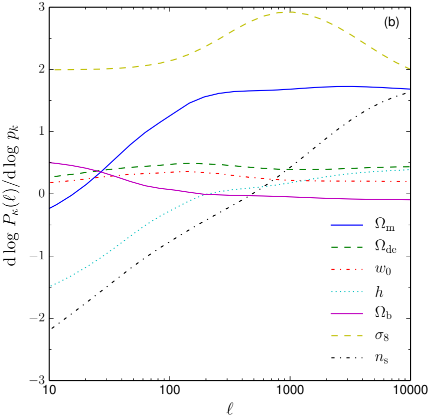

Correlations of two shears I

We have established lensing power spectrum $P_\kappa = P_\gamma$ (power spectrum of projected δ) as interesting quantity for cosmology.

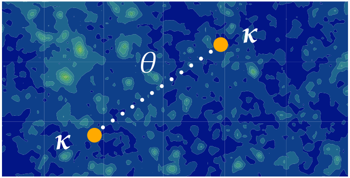

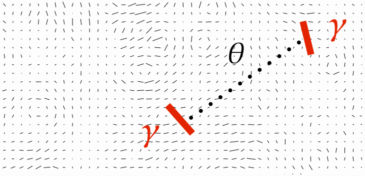

Provides theory model prediction correlation of κ or γ in Fourier space.
However we measure shear (ellipticity) in real space.
Two options to make connection:

1. Fourier-transform data. Square to get power spectrum.
2. Calculate correlations in real space. Inverse-Fourier transorm theory P_κ.

Correlations of two shears II

Correlation of the shear at two points yields four quantities

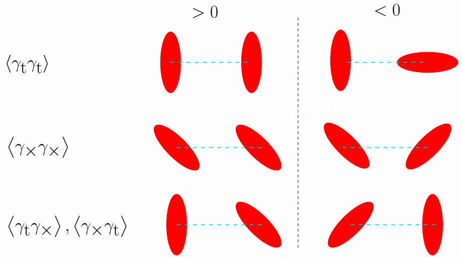

Parity conservation $\longrightarrow \langle\gamma_t\gamma_\times\rangle = \langle\gamma_\times\gamma_t\rangle = 0$

The two components of the shear two-point correlation function (2PCF) are defined as

$$\xi_+(\vartheta) = \langle\gamma_t\gamma_t\rangle(\vartheta) + \langle\gamma_\times\gamma_\times\rangle(\vartheta)$$
$$\xi_-(\vartheta) = \langle\gamma_t\gamma_t\rangle(\vartheta) - \langle\gamma_\times\gamma_\times\rangle(\vartheta)$$

Due to statistical isotropy & homogeneity, these correlators only depend on ϑ.

Correlations of two shears III

The 2PCF is the 2D Fourier transform of the lensing power spectrum.

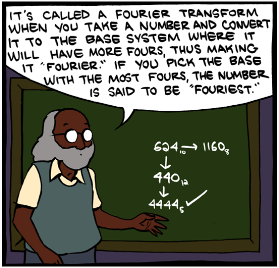

Isotropy → 1D integrals, *Hankel transform.*

$$\xi_+(\vartheta) = \frac{1}{2\pi} \int_0^\infty \mathrm{d}\ell\, \ell \mathrm{J}_0(\ell\vartheta) P_\kappa(\ell)$$
$$\xi_-(\vartheta) = \frac{1}{2\pi} \int_0^\infty \mathrm{d}\ell\, \ell \mathrm{J}_4(\ell\vartheta) P_\kappa(\ell),$$

E- and B-modes I

Shear patterns

We have seen tangential pattern in the shear field due to mass over-densities. Under-dense regions cause a similar pattern, but with opposite sign for γ. That results in radial pattern.

Under idealistic conditions, these are the only possible patterns for a shear field, the E-mode. A so-called B-mode is not generated.

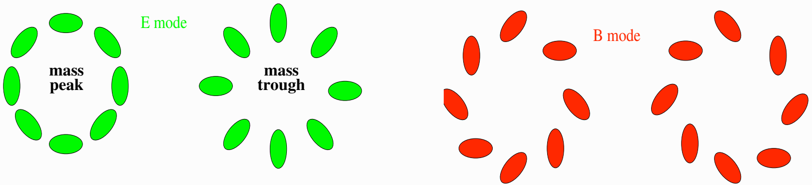

E- and B-modes II

Origins of a B-mode

Measuring a non-zero B-mode in observations is usually seen as indicator of residual systematics in the data processing (e.g. PSF correction, astrometry).

Other origins of a B-mode are small, of %-level:

- Higher-order terms beyond Born appproximation (propagation along perturbed light ray, non-linear lens-lens coupling), and other (e.g. some ellipticity estimators)
- Lens galaxy selection biases (size, magnitude biases), and galaxy clustering
- Intrinsic alignment (although magnitude not well-known!)
- Varying seeing and other observational effects
- Non-standard cosmologies (non-isotropic, TeVeS, . . .)

E- and B-modes III

Measuring E- and B-modes

Separating data into E- and B-mode is not trivial.

To directly obtain $\kappa^{\rm E}$ and $\kappa^{\rm B}$ from γ, there is leakage between modes due to the finite observed field (border and mask artefacts).

One can quantify the shear pattern, e.g. with respect to reference centre points, but the tangential shear $\gamma_{\rm t}$ is not defined at the center.

Solution: filter the shear map. (= convolve with a filter function Q). This also has the advantage that the spin-2 quantity shear is transformed into a scalar.

This is equivalent to filtering κ with a function U that is related to Q.

E- and B-modes IV

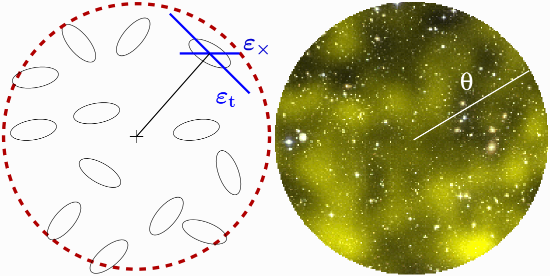

The resulting quantity is called aperture mass $M_{\rm ap}(\theta)$, which is a function of the filter size, or smoothing scale, θ. It is only sensitive to the E-mode.

If one uses the cross-component shear $\gamma_\times$ instead, the filtered quantity, $M_\times$ captures the B-mode contribution only.

End of day 1.

Day 2. Reminder: Overview

Day 1: Principles of gravitational lensing

- Brief history of gravitational lensing
- Light deflection in an inhomogeneous Universe
- Convergence, shear, and ellipticity
- Projected power spectrum
- Real-space shear correlations

Day 2: Measurement of weak lensing

- Galaxy shape measurement
- PSF correction
- Photometric redshifts
- Estimating shear statistics

Day 3: Surveys and cosmology

- Cosmological modelling
- Results from past and ongoing surveys (CFHTLenS, KiDS, DES)
- Euclid

Day 3+: Extra stuff

- Cluster lensing; nature of DM; tests of GR

The shape measurement challenge

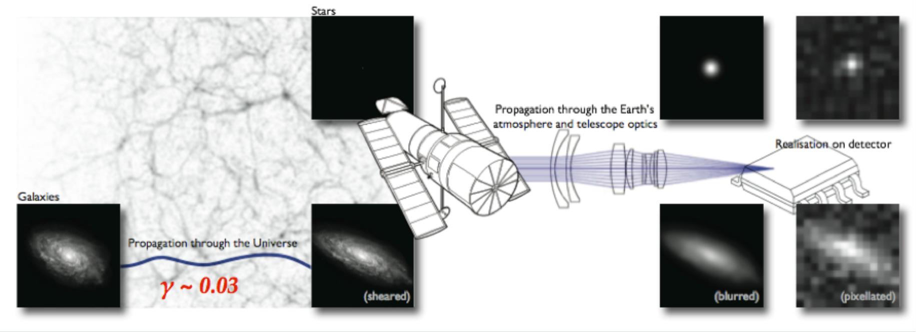

Bridle et al. 2008, great08 handbook

- Cosmological shear $\gamma \ll \varepsilon$ intrinsic ellipticity
- Galaxy images corrupted by PSF
- Measured shapes are biased

The shape measurement challenge

How do we measure "ellipticity" for irregular, faint, noisy, blended objects?

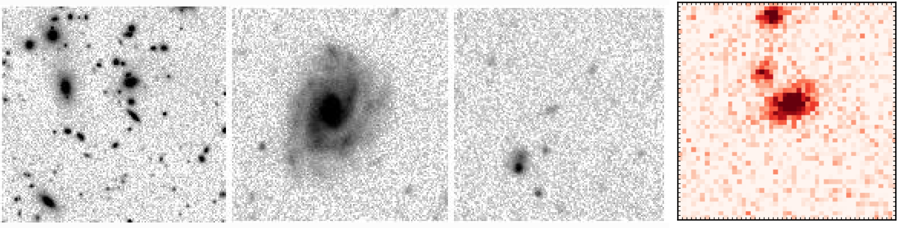

CFHT [(from Y. Mellier)] — DES-SV (Jarvis et al. 2016)

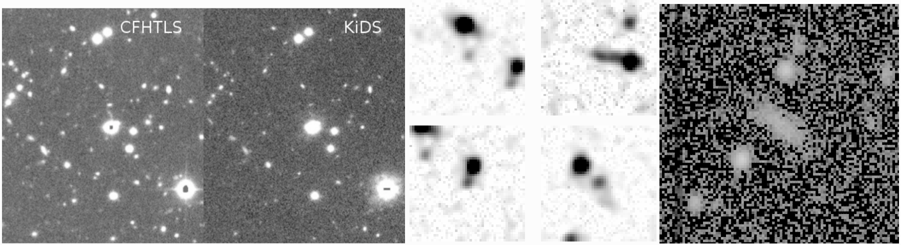

CFHTLenS/KiDS — CFHTLenS (Miller et al. 2013) — DES-Y1 (?)

Shape measurement methods

- Parametric: model fitting.
  (Kuijken 1999), *lens*fit (Miller et al. 2007)), *gfit* (Gentile et al. 2012), *im3shape* (Zuntz et al. 2013), *ngmix* (Jarvis et al. 2016) and many more.
- Non-parametric: direct estimation.
  - Perturbative: weighted moments.
    KSB — (Kaiser et al. 1995) + many improvements
    DEIMOS — (Melchior et al. 2011) PSF correction in moment space
    HOLICs — (Okura & Futamase 2009) — Higher-order moments
  - Non-perturbative: decomposition into basis functions.
    shapelets — (Refregier 2003) + many improvements

Model fitting methods

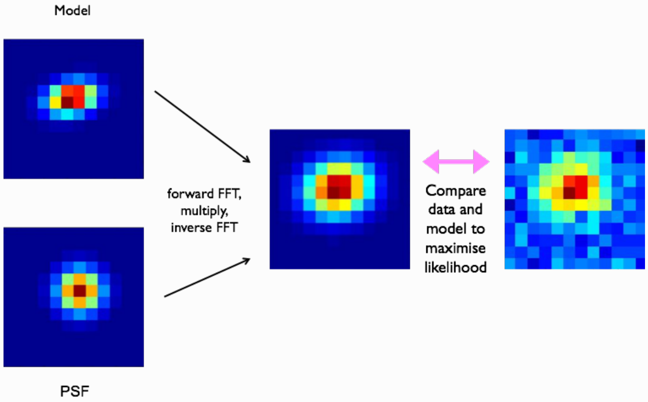

Forward model-fitting (example *lens*fit)

- Convolution of model with PSF instead of devonvolution of image
- Combine multiple exposures (in Bayesian way, multiply posterior density), avoiding co-adding of (dithered) images

Dithering

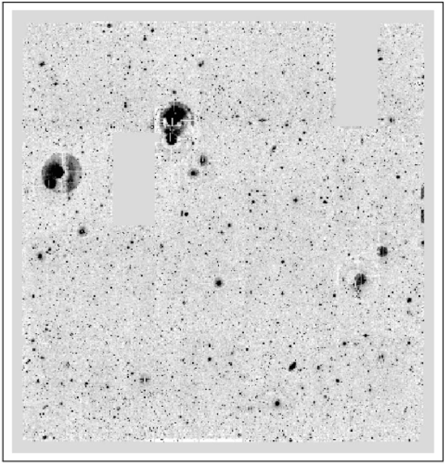

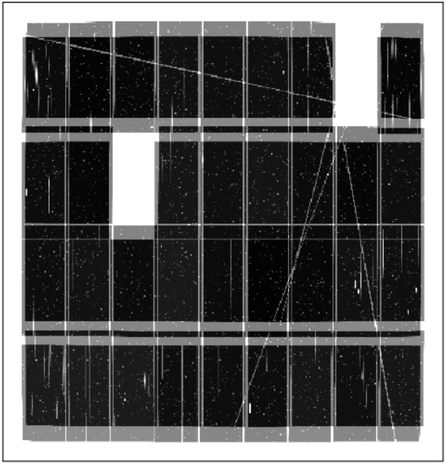

Left: Co-add of two r-band exposures of CFHTLenS.
Right: Weight map.

Moment-based methods I

Moments and ellipticity

How are moments connected to ellipticity?
Q: Simple case: qualitatively, what are the $0^{\rm th}, 1^{\rm st}, 2^{\rm nd}$ moments of a 1D distribution? Of a 2D distribution?
Quadrupole moment of weighted light distribution $I(\boldsymbol{\theta})$:

$$Q_{ij} = \frac{\int \mathrm{d}^2\theta \, q[I(\boldsymbol{\theta})] \, (\theta_i - \bar\theta_i)(\theta_j - \bar\theta_j)}{\int \mathrm{d}^2 \, \theta \, q[I(\boldsymbol{\theta})]}, \quad i, j = 1, 2$$

q : weight function

$$\bar{\boldsymbol{\theta}} = \frac{\int \mathrm{d}^2\theta \, q_I[I(\boldsymbol{\theta})] \, \boldsymbol{\theta}}{\int \mathrm{d}^2\theta \, q_I[I(\boldsymbol{\theta})]} : \quad \text{barycenter (first moment!)}$$

Ellipticity

$$\varepsilon = \frac{Q_{11} - Q_{22} + 2\mathrm{i}Q_{12}}{Q_{11} + Q_{22} + 2(Q_{11}Q_{22} - Q_{12}^2)^{1/2}}$$

Circular object $Q_{11} = Q_{22}, Q_{12} = Q_{21} = 0$

Moment-based methods II

KSB PSF correction

Perturbative ansatz for PSF effects

$$\varepsilon^{\rm obs} = \varepsilon^{\rm s} + P^{\rm sm}\varepsilon^* + P^{\rm sh}\gamma$$

[c.f. $\varepsilon^{\rm obs} = \varepsilon^{\rm s} + \gamma$ from before]

$P^{\rm sm}$	smear polarisability, (linear) response of to ellipticity to PSF anisotropy
e^*	PSF anisotropy
$P^{\rm sh}$	shear polarisability, isotropic seeing correction
γ	shear

$P^{\rm sm}, P^{\rm sh}$ are functions (2×2 tensors) of galaxy brightness distribution.

Problematic: Strongly anisotropic PSF, error estimation, combining multiple exposures.

Non-perturbative methods

Shapelets

(Refregier 2003, Massey & Refregier 2005, Kuijken 2006)

- Decompose galaxies and stars into basis functions.

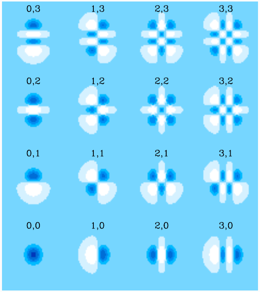

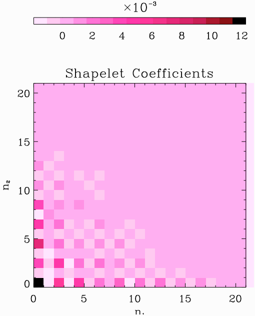

- PSF correction, convergence and shear acts on shapelet coefficients, deconvolution feasible
- Problems: series truncation, basis functions not representative, need to set size parameter

Further methods and techniques

- Generic approaches of shape estimation and/or calibration (can be used together with many shape-measurement methods)
  - Machine-Learning, e.g. LUT by supervised learning, (Tewes et al. 2012)
  - Self-calibration (Fenech Conti et al. 2017)
  - MetaCalibration (**?**, **?**)
- Further Bayesian methods
  - Hierarchical Multi-level Bayesian Inference (MBI), (Schneider et al. 2014). Joint posterior of shear, galaxy properties, PSF, nuisance parameters given pixel data.
  - (Bernstein & Armstrong 2014). Does not measure ellipticity of individual galaxies, direct posterior estimation of shear for population. Needs prior from deep images.

Shear measurement biases: Origin

- **Noise bias**
  In general, ellipticity is non-linear in pixel data (e.g. normalization by flux). Pixel noise $\rightarrow$ biased estimators.
- **Model bias**
  Assumption about galaxy light distribution is in general wrong.
  - Model-fitting method: wrong model
  - Perturbative methods (*KSB, DEIMOS, HOLICS*): weight function not appropriate
  - Non-perturbative methods (*shapelets*): truncated expansion, bad eigenfunction representation
  - Color gradients
  - Non-elliptical isophotes
- **Other**
  - Imperfect PSF correction
  - Detector effects (CTI — charge transfer inefficiency)
  - Selection effects (probab. of detection/sucessful ε measurement depends on ε and PSF)

Shear measurement biases: Characterisation

Bias can be multiplicative ($\boldsymbol{m}$) and additive ($\boldsymbol{c}$):

$$\gamma_i^{\rm obs} = (1 + m_i)\gamma_i^{\rm true} + c_i; \quad i = 1, 2.$$

Biases $\boldsymbol{m}$, $\boldsymbol{c}$ are typically complicated functions of galaxy properties (e.g. size, magnitude, ellipticity), redshift, PSF, ... They can be scale-dependent.

Current methods: $|m| = 1\% - 10\%, |c| = 10^{-3} - 10^{-2}$.

Challenges such as STEP1, STEP2, great08, great10, great3 quantified these biases with blind simulationes.

Requirements

Normalisation $\sigma_8 \propto m$!
Necessary knowledge of residual biases $|\Delta m|, |\Delta c|$ (after calibration):
Current surveys 1%.
Future large missions (Euclid, LSST, ...) $10^{-4} = 0.1\%$!

Shear measurement biases: Calibration

Usually biases are calibrated using simulated or emulated data, or the data (self-calibration, metacalibration) themselves.
Current surveys typicall produce corresponding image simulations with matching properties of galaxy sample, selection, and PSF matching to data.

Functional dependence of m on observables must not be too complicated (e.g. not smooth, many variables, large parameter space), or else measurement is *not calibratable*!

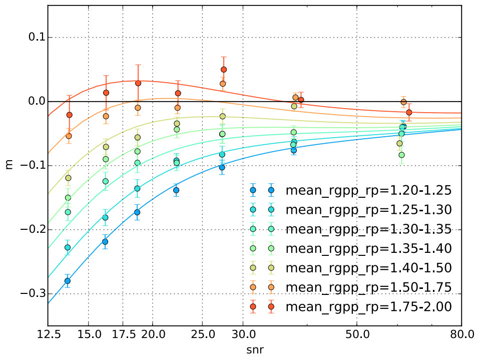

(Jarvis et al. 2016)

PSF correction

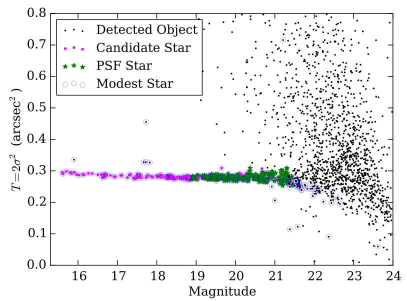

(Jarvis et al. 2016)

- Select clean sample of stars
- Measure star shapes
- Create PSF model and interpolate (pixel values, ellipticity, PCA coefficients, ...) to galaxy positions. Space-based observations: global PSF model from many exposures possible
- Correct for PSF: galaxy image devonvolution or other (e.g. linearized) correction, or convolve model

PSF correction

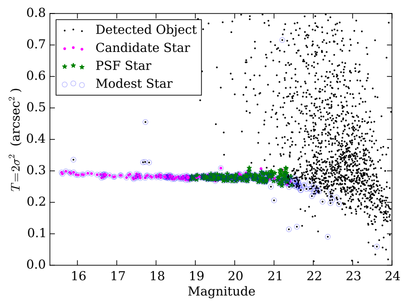

(Jarvis et al. 2016)

- Select clean sample of stars
- Measure star shapes
- Create PSF model and interpolate (pixel values, ellipticity, PCA coefficients, ...) to galaxy positions. Space-based observations: global PSF model from many exposures possible
- Correct for PSF: galaxy image devonvolution or other (e.g. linearized) correction, or convolve model

PSF correction

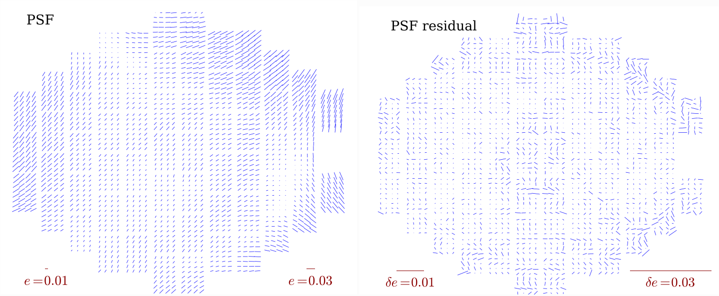

(Jarvis et al. 2016)

- Select clean sample of stars
- Measure star shapes
- Create PSF model and interpolate (pixel values, ellipticity, PCA coefficients, ...) to galaxy positions. Space-based observations: global PSF model from many exposures possible
- Correct for PSF: galaxy image devonvolution or other (e.g. linearized) correction, or convolve model

PSF correction

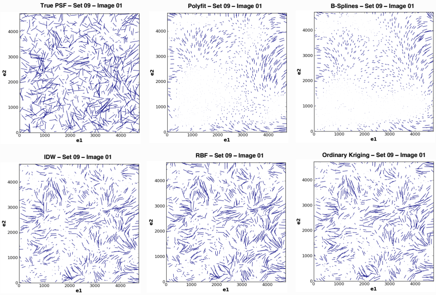

(Gentile et al. 2013)

- Select clean sample of stars
- Measure star shapes
- Create PSF model and interpolate (pixel values, ellipticity, PCA coefficients, ...) to galaxy positions. Space-based observations: global PSF model from many exposures possible
- Correct for PSF: galaxy image devonvolution or other (e.g. linearized) correction, or convolve model

PSF correction

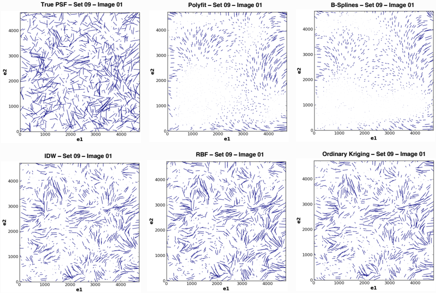

(Gentile et al. 2013)

- Select clean sample of stars
- Measure star shapes
- Create PSF model and interpolate (pixel values, ellipticity, PCA coefficients, ...) to galaxy positions. Space-based observations: global PSF model from many exposures possible
- Correct for PSF: galaxy image devonvolution or other (e.g. linearized) correction, or convolve model

Quantifying PSF residuals I

Null test: $\xi_{\rm sys}$ correlation between star and galaxy shapes expected to vanish, unless PSF correction (using stars to correct galaxy shapes) is not perfect.

$$\xi_{\rm sys} = \langle \varepsilon^* \varepsilon \rangle$$

This measures residual PSF pattern leakage onto galaxy field.
Caveat: LSS can show chance alignments with PSF pattern. Sample or *cosmic variance* has to be accunted for → N-body simulations!

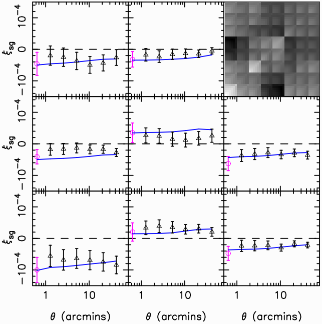

(Heymans et al. 2012)

Quantifying PSF residuals II

Histogram of probability p that $\Sigma\xi_{\rm obs} \sim \Sigma|\xi_{\rm sys}|$ is not zero (sum over all pointings), from simulations.

Shaded region = data.

Magenta: simulations without LSS.

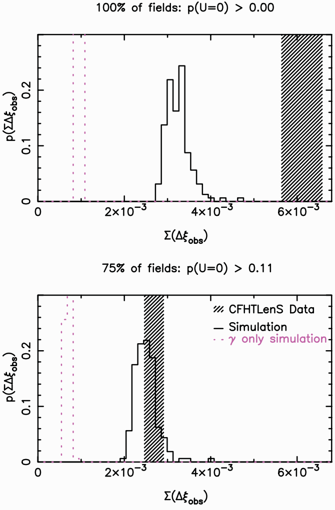

[Heymans et al. 2012, CFHTLenS]

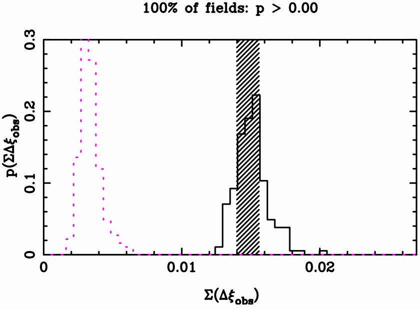

[Hildebrandt et al. 2016, KiDS-450]

Redshift estimation I

Redshifted galaxy spectra have different colors.
Photometric redshifts = very low resolution spectra.
#bands between 3 (RCS) and 30 (COSMOS). Typical are 4-5 optical filters (g, r, i, y, z), maybe with UV (u) and IR (I, J, K).

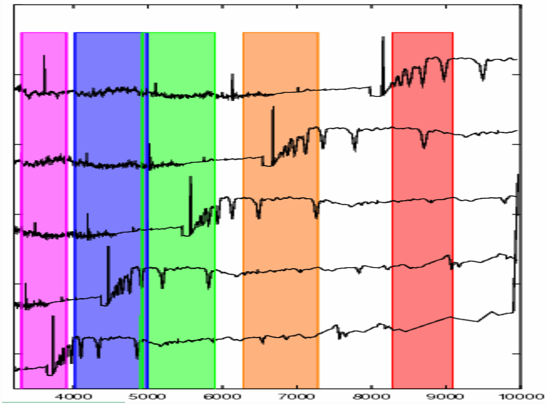

[from Y. Mellier]

4000 Å-break strongest feature → ellipticals (old stellar population) best, spirals ok, irregular/star-burst (emission lines) more unreliable.

Redshift estimation II

Properties

- Redshift desert $z \approx 1.5 - 2.5$, neither 4000 Å-break nor Ly-break in visible range, very hard to access from ground.
- Confusion between low-z dwarf ellipticals and high-z galaxies. Confusion between Balmer and Lyman break. Catastrophic outliers, typically a few to a few 10
- Need UV band and IR for high redshifts! But: UV very inefficient, IR absorbed by atmosphere, have go to space.
- Need spectroscopic galaxy sample for comparison, calibration, or cross-correlation. In general $N_{\rm spec} \ll N_{\rm WL}$.
- Typical accuracy of photo-z's $\sigma/(1+z) \sim 0.05$ (depending on filters).

Redshift estimation III

Redshift accuracy and cosmology

To interpret weak lensing correlations in cosmological context, the redshift distribution needs to be known accurately!
To first order:

$$P_\kappa(\ell \sim 1000) \propto \Omega_{\rm de}^{-3.5} \sigma_8^{2.9} \bar{z}^{1.6} |w|^{0.31} \quad \text{(Huterer et al. 2006)}$$

Methods

- Template fitting.
  Redshifted synthetic or observed templates of various types are fitted to flux in observed bands.
  Examples *LePhare* (Ilbert et al. 2006)), *BPZ* (Benítez 2000), *HyperZ* (Bolzonella et al. 2000).
  Spectroscopic sample for calibration, priors.
- Machine-learning.
  Learn data using training set (of spectroscopic sample).
  Examples: *ANNz* (Collister & Lahav 2004).

Redshift estimation IV

- Matching photometric properties to spectroscopic sample (Lima et al. 2008) (direct calibration).
- Spatial cross-correlation with spectroscopic survey (clustering redshifts)

Spectroscopic sample has to be representative in some properties, depending on the method:

- Template fitting: Same magnitude limit as photometric sample
- Neural networks: Cover redshift range, properties (colors)
- Matching: Cover (color) parameter space
- Clustering: Cover redshift range, sky overlap

Clustering redshifts (slide from Vivien Scottez)

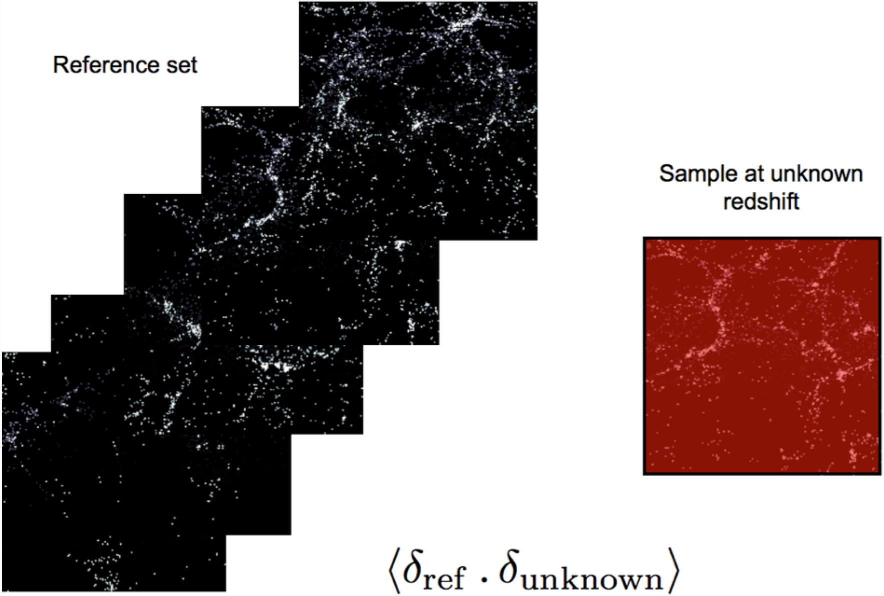

$$\langle \delta_{\mathrm{ref}} \cdot \delta_{\mathrm{unknown}} \rangle$$

Estimator of second-order functions I

Remember the shear two-point correlation function (2PCF)?

$$\xi_\pm(\vartheta) = \langle \gamma_\mathrm{t}\gamma_\mathrm{t} \rangle (\vartheta) \pm \langle \gamma_\times\gamma_\times \rangle (\vartheta)$$

Unbiased estimator of $\xi_\pm$ just involves sums over galaxy pairs:

$$\hat{\xi}_\pm(\theta) = \frac{\sum_{ij} w_i w_j \left(\varepsilon_{\mathrm{t},i}\varepsilon_{\mathrm{t},j} \pm \varepsilon_{\times,i}\varepsilon_{\times,j} \right)}{\sum_{ij} w_i w_j}.$$

Sum over galaxy pairs with angular distance within bin of θ.

- Unbiased estimator (for bin size $\to 0$, and in absence of intrinsic alignment)
- No need for random catalogue, or mask geometry, since $\xi = 0$ in absence of lensing.
- No need to pixellise data, can use brute-force or tree codes/linked lists (adaptive pixellisation, effective smoothing)

Estimator of second-order functions II

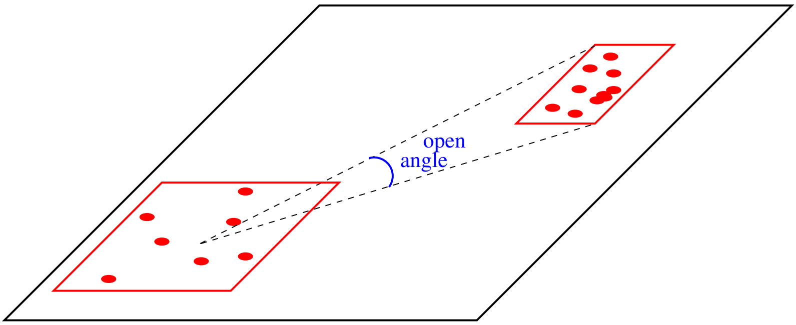

Tree code: correlating two 'nodes' (2D regions).

Estimator of second-order functions III

From the 2PCF estimator, the aperture-mass dispersion and other second-order functions can be derived:

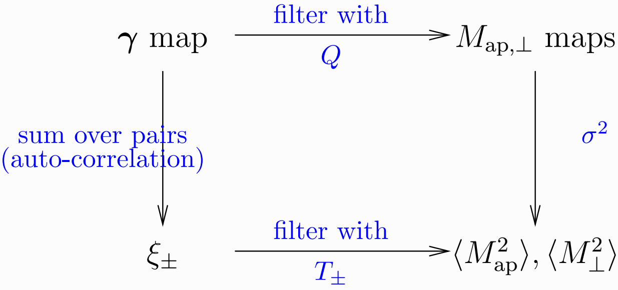

Estimator of second-order functions IV

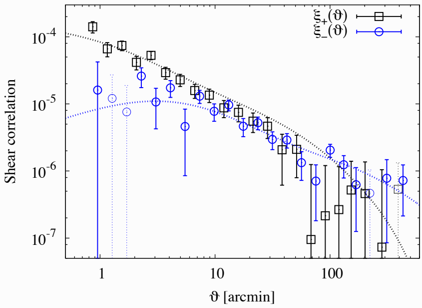

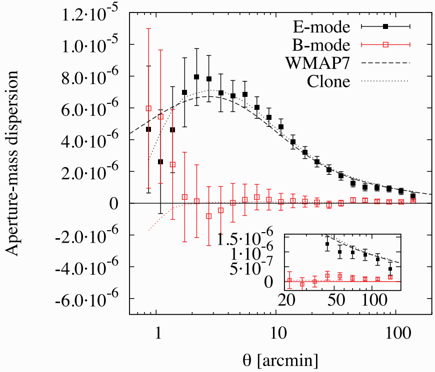

(Kilbinger et al. 2013)

End of day 2.

Day 3. Reminder: Overview

Intrinsic galaxy alignment (IA)

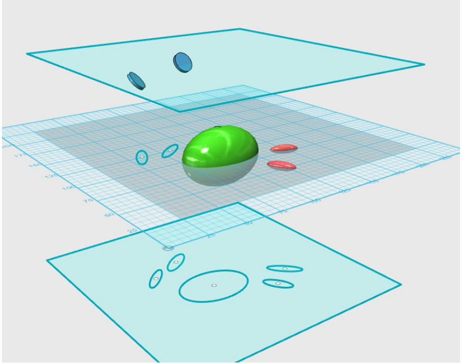

(Joachimi et al. 2015)

Galaxy shapes are correlated with surrounding tidal density field, due to coupling of spins for spiral galaxies, tidal stretching for elliptical galaxies.
Shape of galaxies is sum of shear (G) and intrinsic (I) shape (remember $\varepsilon \approx \varepsilon^{\rm s} + \gamma$).
So, with intrinsic alignment, the correlation of galaxy shapes is not only shear-shear (GG), but also intrinsic-intrinsic (II) and shear-intrinsic (GI; (Hirata & Seljak 2004)).

Contamination to cosmic shear at ~ 1 - 10%.
Need to model galaxy formation.

IA measurement: Ellipticity - density correlations

With (spectroscopic) data measure γ_t around massive galaxies (= centres of halos): shape - density correlations.

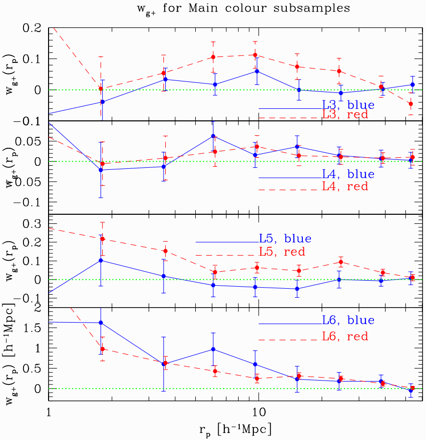

(Hirata et al. 2007)

IA measurement: Ellipticity - ellipticity correlations

With photometric data measure sum of GG, GI, and II.

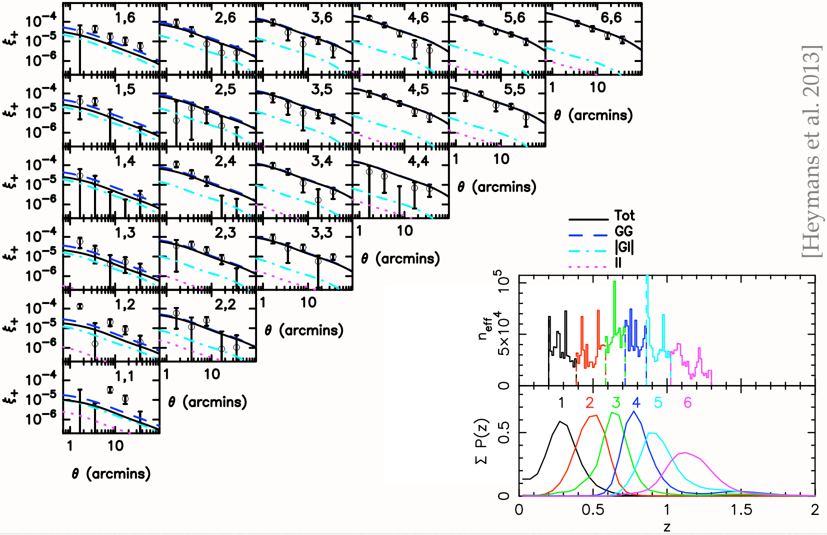

[Heymans et al. 2013]

IA constraints

Simple intrinsic alignment model:
Galaxy ellipticity linearly related to tidal field
[Hirata & Seljak 2004, Bridle & King 2007].

One free amplitude parameter A, fixed z-dependence.

A = 1: reference IA model.
A = 0: no IA

$$A_{\rm late} = 0.18^{+0.83}_{-0.82}$$

$$A_{\rm early} = 5.15^{+1.74}_{-2.32}$$

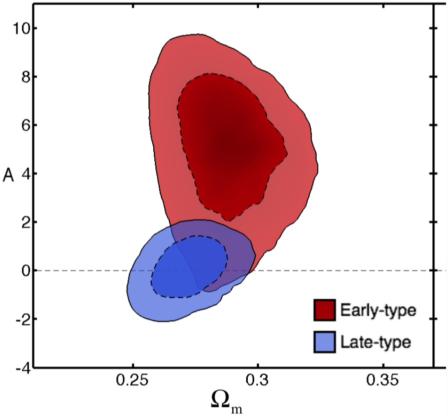

[Heymans et al. 2013]

Baryons in the LSS

On small (halo) scales, dark-matter only models do not correctly reproduce clustering:

- $R \sim 1$ - 0.1 Mpc: gas pressure $\rightarrow$ suppression of structure formation, gas distribution more diffuse wrt dm
- $R < 0.1$ Mpc ($k > 10$/Mpc): Cooling, AGN+SN feedback $\rightarrow$ baryons condense & form stars & galaxies, increase of density & clustering

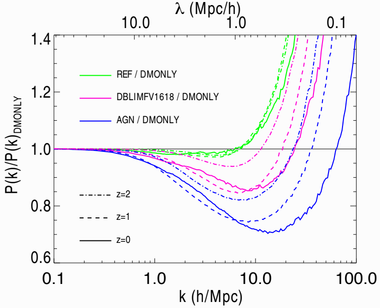

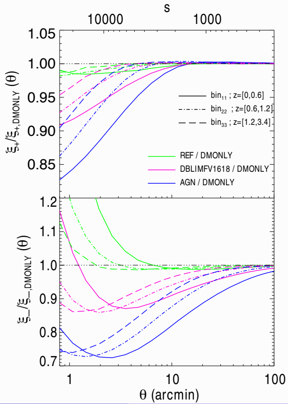

(Semboloni et al. 2011)

CFHTLS/CFHTLenS

Observations 2003 – 2008

Publications 2006 – 2017, peak 2013–2014

Groundbreaking for weak cosmological lensing:

- MegaCam 1 $\deg^2$ fov (@ 3.6m CFHT)
- Multiple optical bands → photometric redshifts, tomography
- Large team (> 20; led by Yannick Mellier, Catherine Heymans, Ludovic van Waerbeke), thorough testing, multiple pipelines
- Public release of all data and lensing catalogues (`www.cfhtlens.org`)

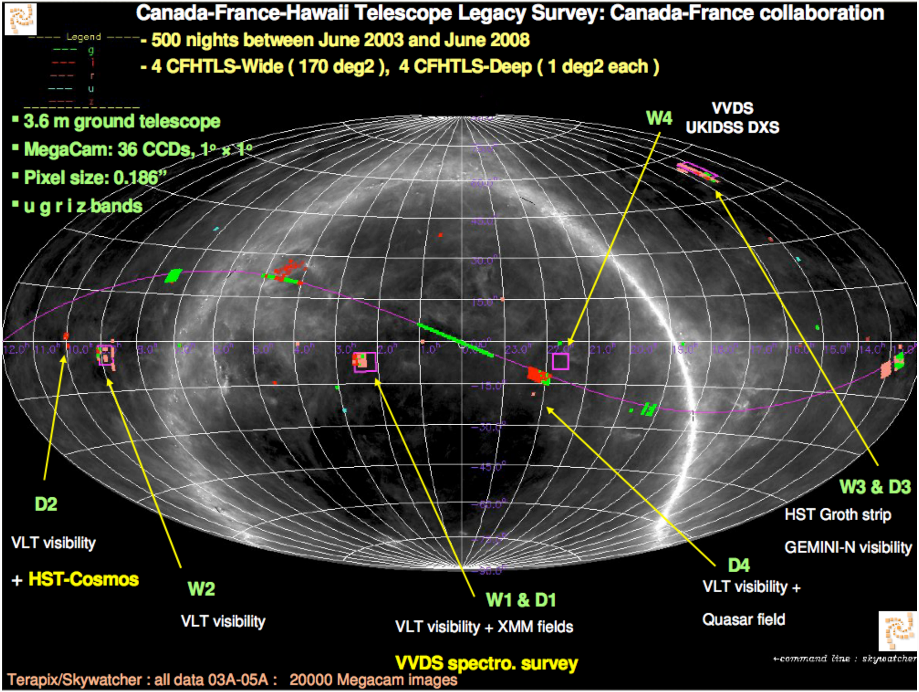

Canada-France-Hawaii Telescope Legacy Survey: Canada-France collaboration
Legend
g
i
r
u
z
- 500 nights between June 2003 and June 2008
- 4 CFHTLS-Wide (170 deg2), 4 CFHTLS-Deep (1 deg2 each)
▪ 3.6 m ground telescope
▪ MegaCam: 36 CCDs, 1° x 1°
▪ Pixel size: 0.186"
▪ u g r i z bands
W4
VVDS
UKIDSS DXS
W3 & D3
HST Groth strip
GEMINI-N visibility
D2
VLT visibility
+ HST-Cosmos
W2
VLT visibility
W1 & D1
VLT visibility + XMM fields
D4
VLT visibility +
Quasar field
VVDS spectro. survey
Terapix/Skywatcher : all data 03A-05A : 20000 Megacam images
←command line : skywatcher

CFHTLenS cosmological constraints

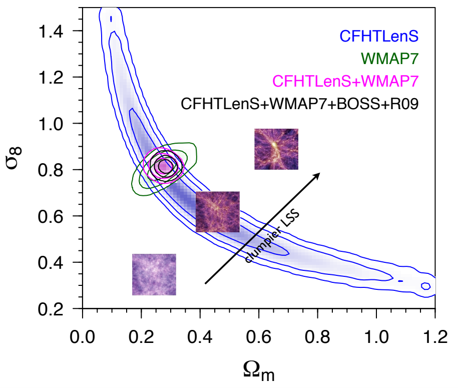

2D lensing
(Kilbinger et al. 2013)

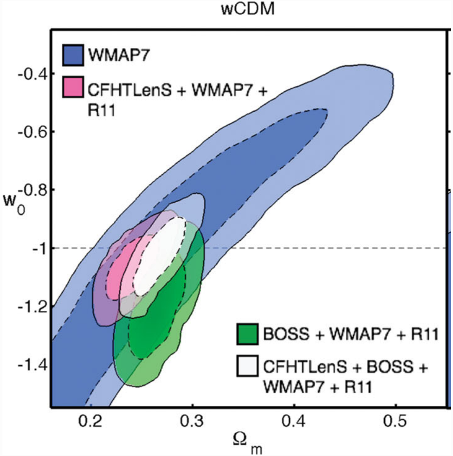

6-bin tomography
(Heymans et al. 2013)

CFHTLenS modified gravity

$$ds^2 = -(1+2\varphi)dt^2 + (1-2\phi)a^2 d\vec{x}^2$$

time dilation — spatial curvature

- Gravitational potential as experienced by galaxies:

$$\nabla^2 \varphi = 4\pi G a^2 \bar{\rho} \delta \left[1 + \mu\right] \qquad \mu(a) \propto \Omega_\Lambda(a)$$

- Gravitational potential as experienced by photons:

$$\nabla^2 (\varphi + \phi) = 8\pi G a^2 \bar{\rho} \delta \left[1 + \Sigma\right] \qquad \Sigma(a) \propto \Omega_\Lambda(a)$$

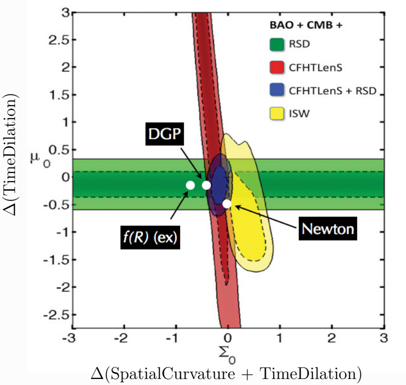

2-bin tomography
(Simpson et al. 2013)

KiDS

Observations 2011 – 2017.
Publications 2016 + 2017: KiDS-450, 1/3 of the final area.

- $1,500$ deg^2 in four optical (+ 5 IR) bands
- New camera (OmegaCAM 1 deg^2 fov) and telecsope (2.6 m VST), long delay
- Compared four different redshift estimation methods

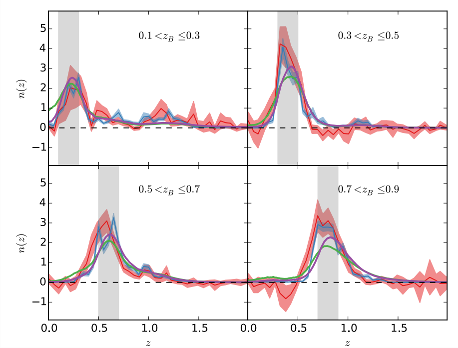

(Hildebrandt et al. 2017)

KiDS

Very thorough weak-lensing analysis, including:

- $n(z)$ errors
- IA, baryonic effects
- Shear calibration
- Non-Gaussian covariance
- Blinded analysis

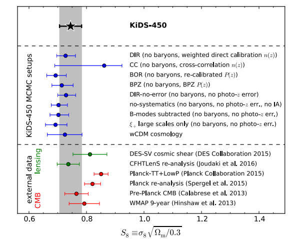

(Hildebrandt et al. 2017)

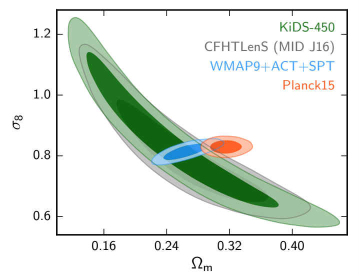

(Hildebrandt et al. 2017)

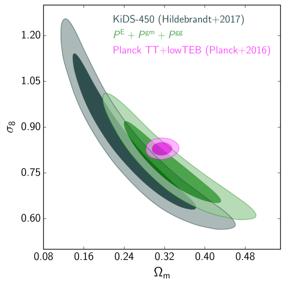

(?)

DES — Dark Energy Survey

Observations 2013 – 2018

- Dedicated new camera: DECam, 3 deg^2 fov, weak lensing as one of four main science experiments
- @ 4m class Blanco telecsope on Cerro Tololo, Chile
- $5,000$ deg^2 when completed
- Large coverage in other wavelength (e.g. SPT)
- 2016: published results Science Verification Data (SVD), 139 $\text{deg}^2 = 3\%$ of final area, but nominal depth and filters
- This summer (2017): published Y1 (year one) data, 1321 deg^2 area for lensing

DES — cosmological constraints

SPV 2016

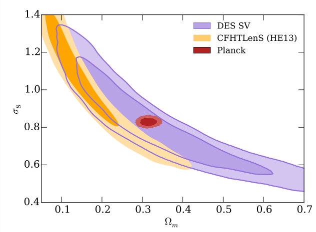

(The Dark Energy Survey Collaboration et al. 2016)

Y1 2017

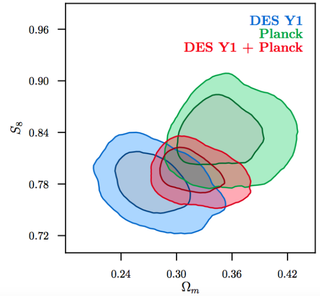

(?)

Y1 2017

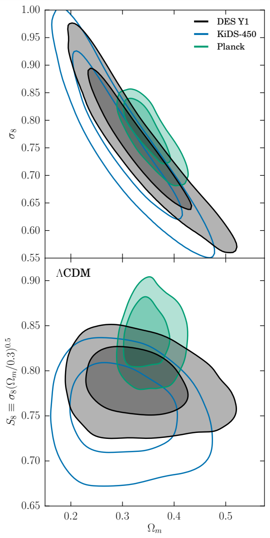

(?)

Summary

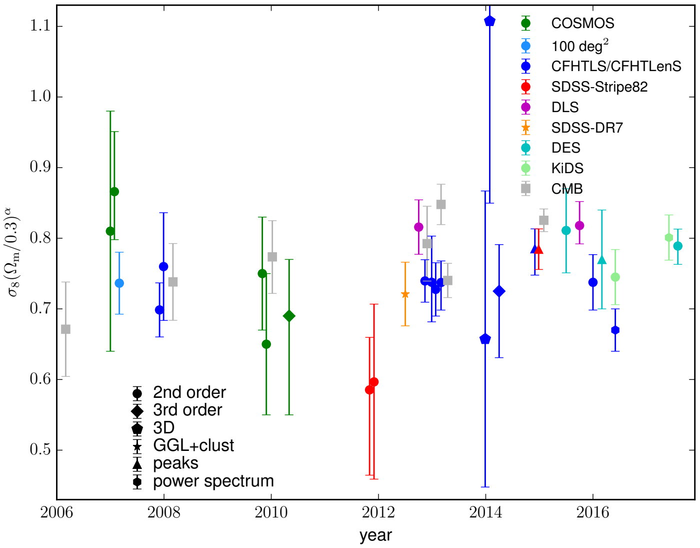

COSMOS
100 deg^2
CFHTLS/CFHTLenS
SDSS-Stripe82
DLS
SDSS-DR7
DES
KiDS
CMB
2nd order
3rd order
3D
GGL+clust
peaks
power spectrum
$\sigma_8(\Omega_{\rm m}/0.3)^\alpha$
year
2006
2008
2010
2012
2014
2016
0.5
0.6
0.7
0.8
0.9
1.0
1.1

Discrepancy with Planck?

- Maybe not (2 - 3σ). However, also discrepancy of CMB C_ℓ's with SZ cluster counts.
- Additional physics, e.g. massive neutrinos? Not sufficient evidence.
- WL systematics? (E.g. shear bias, baryonic uncertainty on small scales.) KiDS say not likely.
- DES closer to Planck.
- Adding clustering and galaxy-galaxy lensing moves normalisation closer to Planck.

The Euclid mission

Why is Euclid so special and challenging?
Increase of factor 100 in data volume compare to current surveys!
Few Million to few 100 Million galaxies.

For 2PCF: Naive increase of $n_{\rm correl}$ by $10,000$!

Comparison with Planck:
Planck all-sky, pixel size ~ 7 arc min.
Euclid 1/3 sky, pixel size $\sim$ typical angular distance between galaxies $\sim$ arc sec.
Factor 10^5 more pixels!

Weak-lensing resolution

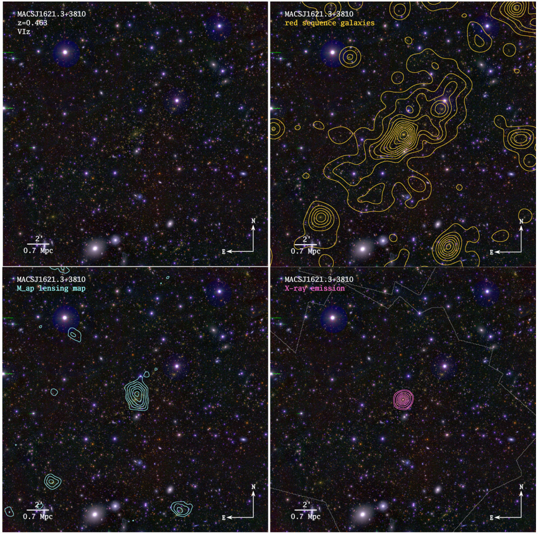

(von der Linden et al. 2014) — MACS_J1621+3810, ground-based data, $n_{\rm gal} = 2.5 \ldots 25$ arcmin^{-2}

Weak-lensing resolution

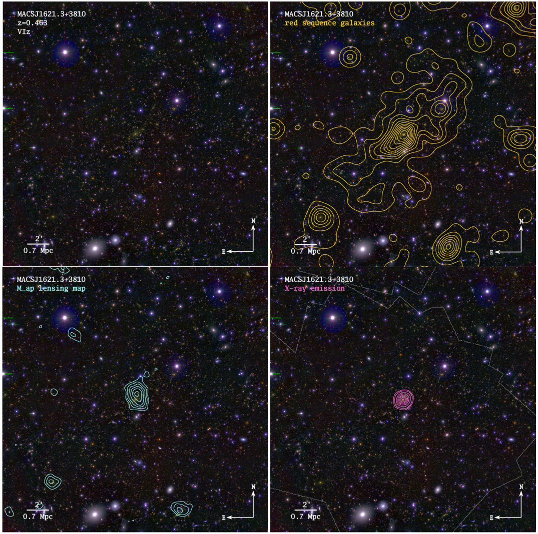

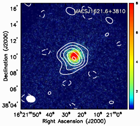

(Bonamente et al. 2012) — X- and SZ

Weak-lensing resolution

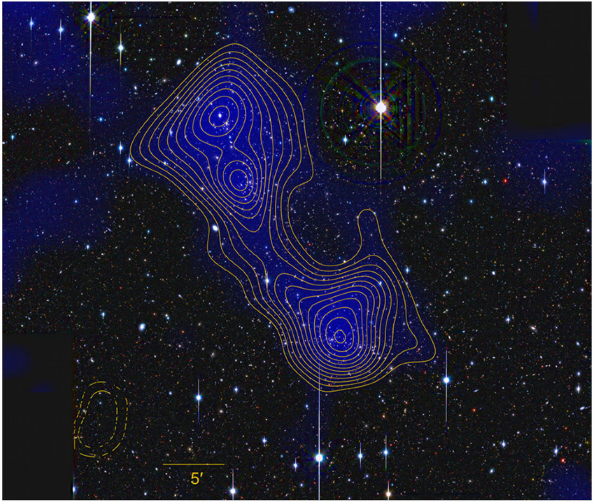

A 222/223, filament between clusters (Dietrich et al. 2012)

Mass maps from CFHTLenS

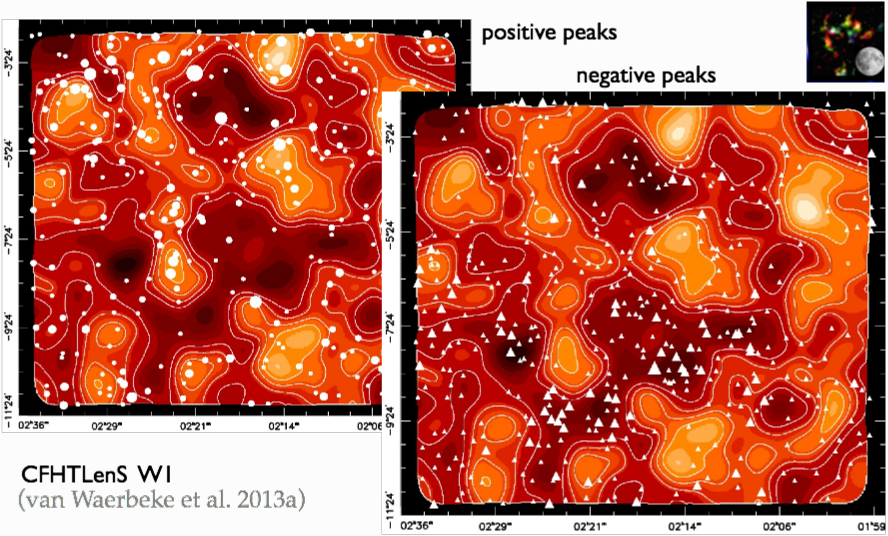

CFHTLenS W1
(van Waerbeke et al. 2013a)

Euclid imaging

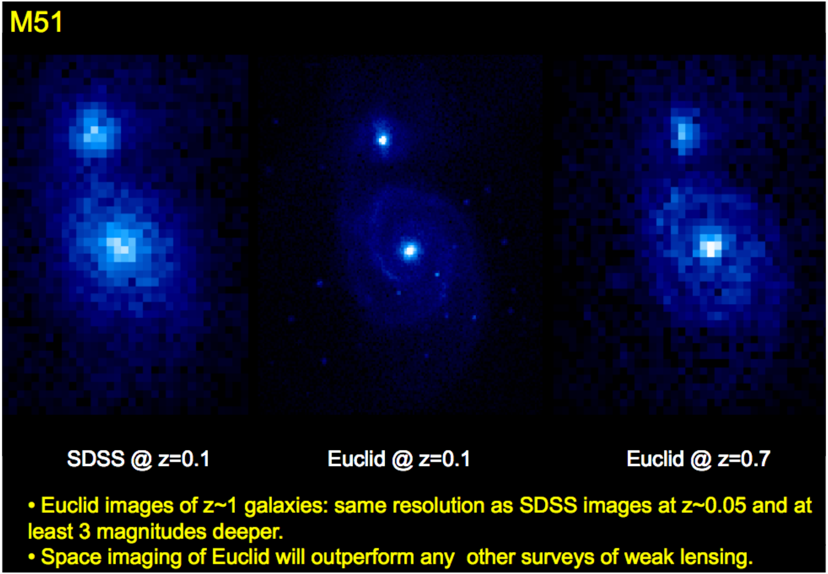

Some Euclid WL challenges

under-sampled PSF

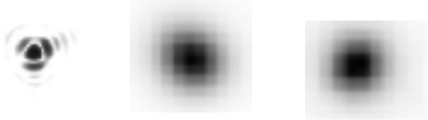

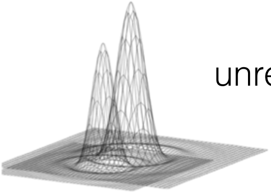

unresolved binary stars

CTI
(charge transfer inefficiency)

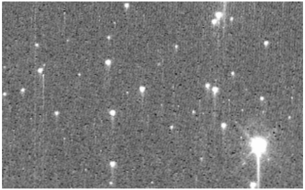

color gradients

Open questions (selection) I

Modelling

- Intrinsic alignment. Dependence on L, type, z? Physically motivated model. N-body simulations.

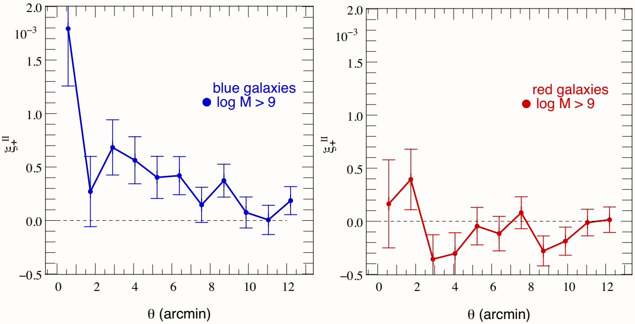

(Codis et al. 2015)

Open questions (selection) II

- IA contamination depends on shape measurement method!

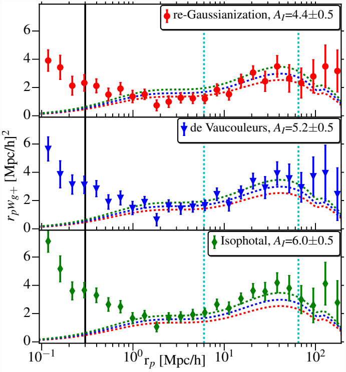

(Singh & Mandelbaum 2016)

- Baryonic feedback in clusters, influence on WL, modelling.

Open questions (selection) III

Photometric redshifts

- Euclid needs (very deep!) ground-based follow-up in multiple optical bands. Data (DES, KiDS, CFIS, ...) will be inhomogeneous. Problem of reliable photo-z's not yet solved.

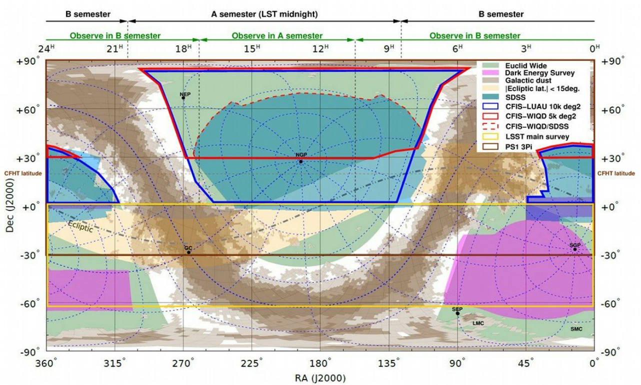

Further possible topics

1. Cluster weak lensing
2. Nature of dark matter (bullet cluster)
3. Testing GR with WL and galaxy clustering
4. Higher-order statistics: peak counts

Stacked cluster weak lensing: Large scales

Weak lensing measures mass associated with clusters.

At large distances: excess mass in nearby, correlated clusters
→ clustering of galaxy clusters.

bg shear - fg position $\sim b_\mathrm{h} \sigma_8^2$

halo bias, function of mass

1200 clusters in 150 deg² CFHTLenS area, $0.1 < z < 0.6$ (mean $z = 0.37$).

Covone, Sereno, MK & Cardone (2014)

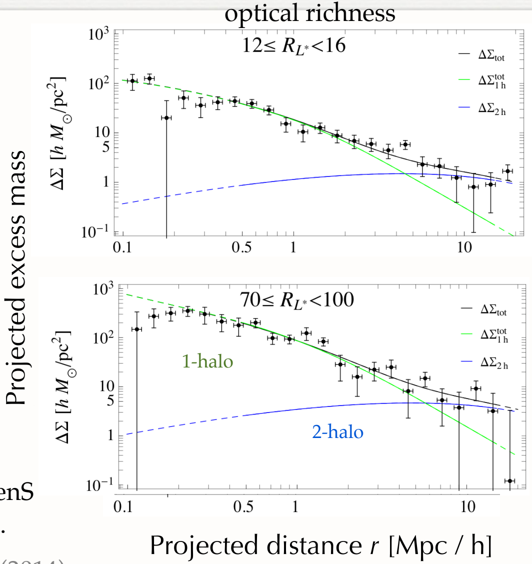

Stacked cluster weak lensing: 2D mass profiles

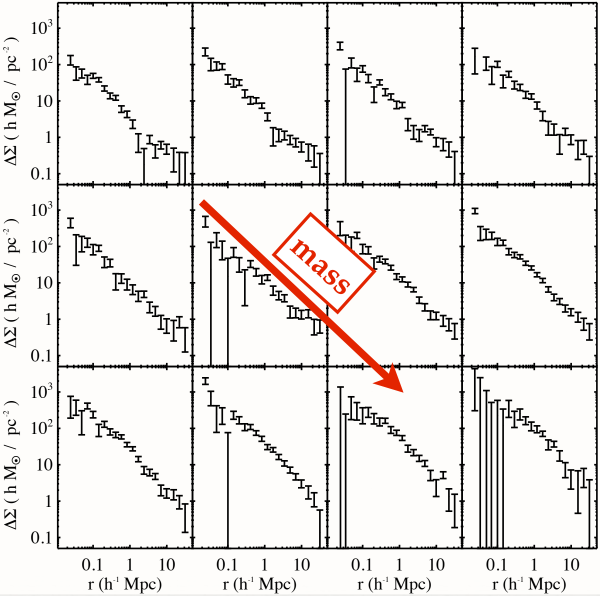

Bin number	N_{200}
1	3
2	4
3	5
4	6
5	7
6	8
7	9-11
8	12-17
9	18-25
10	26-40
11	41-70
12	71-220

130,000 clusters in of SDSS ~ 6,000 deg^2 at z=0.25

Johnston et al. (2009)

Stacked cluster weak lensing: Scaling relations

Covone et al. (2014)

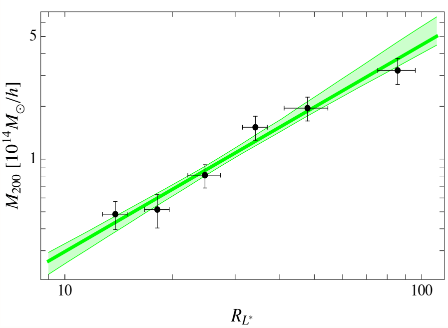

Johnston et al. (2009)

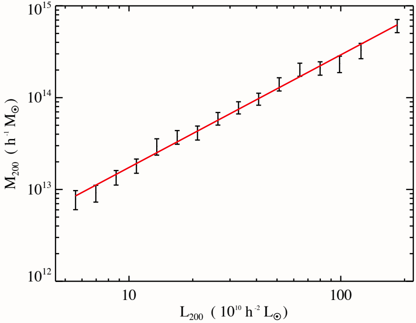

- Scaling relations, necessary calibrating (mass - observable) for cosmology
- XXL (M. Pierre): ~ 100 X-ray selected clusters, 25 deg^2 overlap with CFHTLS, compare lensing and X-ray derived masses.

Stacked cluster weak lensing on large scales

Covone et al. (2014)

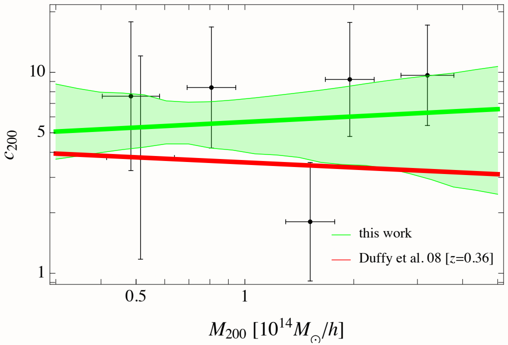

Johnston et al. (2009)

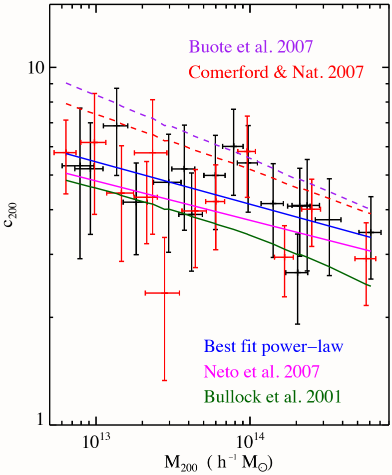

- Concentration parameter c reflects central halo density; depends on assembly history, formation time
- Predictions usually from N-body simulations
- Indirect test of CDM paradigm

The bullet cluster and the nature of dark matter

The bullet cluster

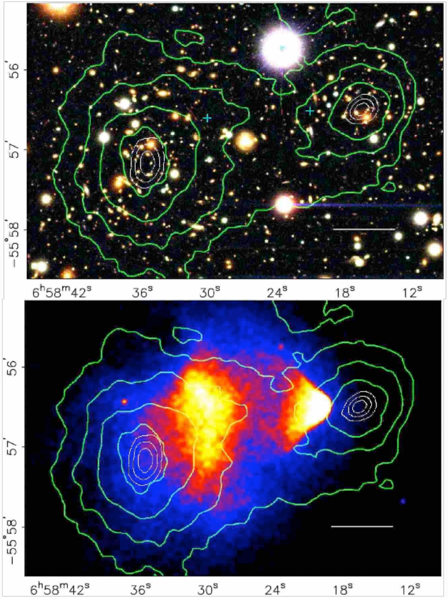

Clowe et al. (2006)

- Merging galaxy cluster at $z = 0.296$
- Recent major merger 100 Myr ago
- Components moving nearly perpendicular to line of sight with $v = 4700$ km s^{-1}
- Galaxy concentration offset from X-ray emission. Bow shocks visible

The bullet cluster: SL+WL measurements

Instrument	Date of Obs.	FoV	Passband	$t_{\rm exp}$ (s)	$m_{\rm lim}$	$n_{\rm d}$ ($'^{-2}$)	seeing
2.2m ESO/MPG	01/2004	$34' \times 34'$	R	14100	23.9	15	$0\farcs8$
Wide Field Imager	01/2004		B	6580			$1\farcs0$
	01/2004		V	5640			$0\farcs9$
6.5m Magellan	01/15/2004	$8'$ radius	R	10800	25.1	35	$0\farcs6$
IMACS	01/15/2004		B	2700			$0\farcs9$
	01/15/2004		V	2400			$0\farcs8$
HST ACS	10/21/2004	$3\farcm5\times3\farcm5$	F814W	4944	27.6	87	$0\farcs12$
subcluster	10/21/2004		F435W	2420			$0\farcs12$
	10/21/2004		F606W	2336			$0\farcs12$
main cluster	10/21/2004	$3\farcm5\times3\farcm5$	F606W	2336	26.1	54	$0\farcs12$

(Bradač et al. 2006, Clowe et al. 2006)

The bullet cluster: strong lensing

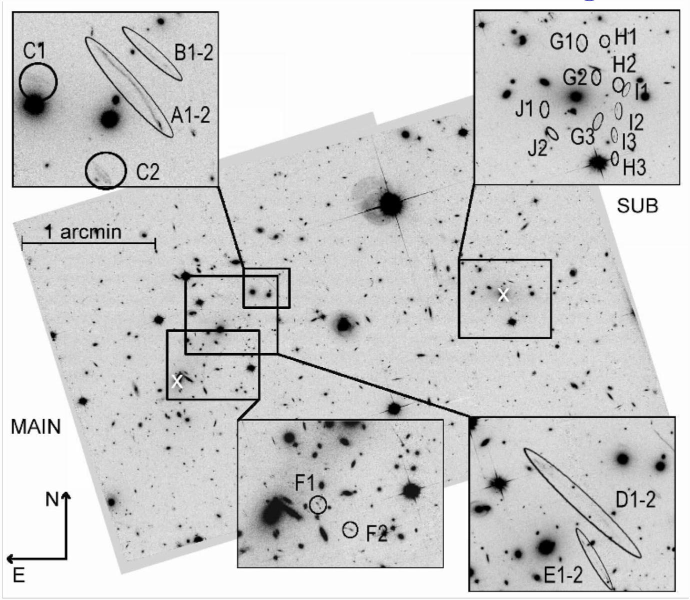

The bullet cluster: WL and X-ray

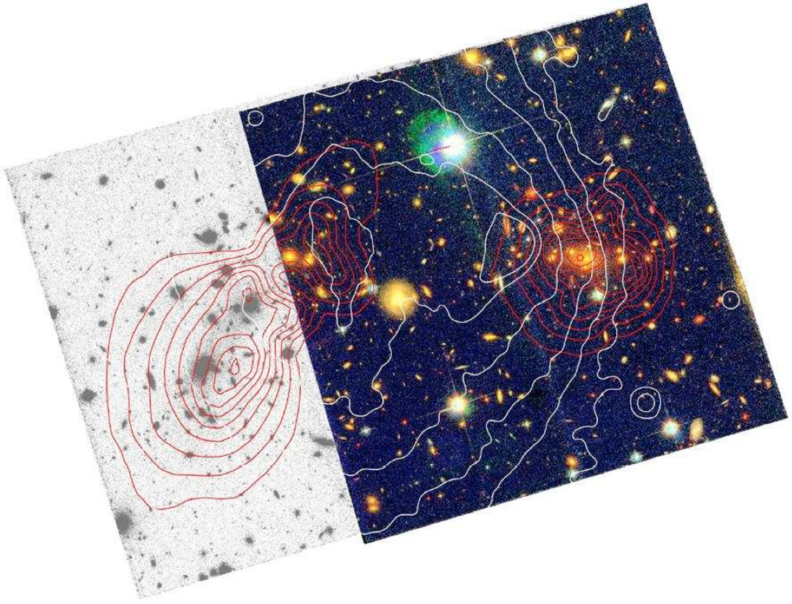

The bullet cluster: Evidence for dark matter

- $10\sigma (6\sigma)$ offset between main (sub-)mass peak and X-ray gas → most cluster mass is not in hot X-ray gas (unlike most baryonic mass: $m_X \gg m_*$!)
- Main mass associated with galaxies → this matter is collisionless

Modified gravity theories without dark matter: MoND (Modified Newtonian Dynamics), (Milgrom 1983), changes Newton's law for low accelerations ($a \sim 10^{-10}$ m s^{-2}), can produce flat galaxy rotation curves and Tully-Fisher relation.
MoND's relativistic version (Bekenstein 2004), varying gravitational constant $G(r)$. Introduces new vector field ("phion") with coupling strenght $\alpha(r)$ and range $\lambda(r)$ as free functions.
This can produce non-local weak-lensing convergence mass, where $\kappa \not\propto \delta$!
Necessary to explain offset between main κ peak and main baryonic mass.
Model with four mass peaks can roughly reproduce WL map with additional collisionless mass! E.g. 2 eV neutrinos.

The bullet cluster: MoND model

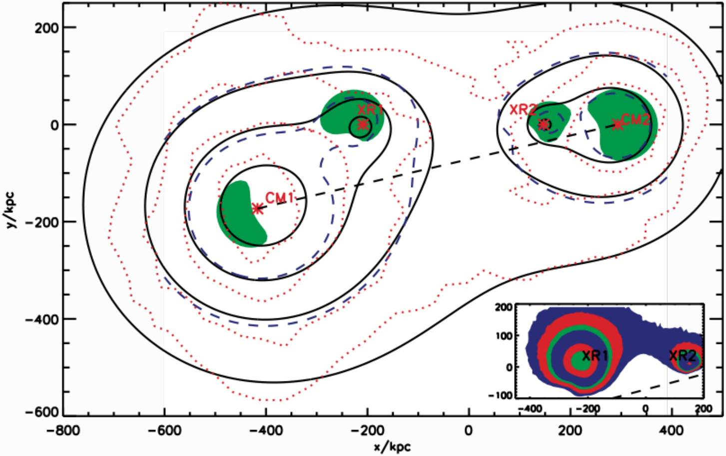

FIG. 1.— Our fitted convergence map (solid black lines) overplotted on the convergence map of C06 (dotted red lines) with x and y axes in kpc. The contours are from the outside 0.16,0.23,0.3 and 0.37. The centres of the four potentials we used are the red stars which are labelled. Also overplotted (blue dashed line) are two contours of surface density [4.8 & 7.2]$\times 10^2 M_\odot$ pc^{-2} for the MOND standard μ function; note slight distortions compared to the contours of κ. The green shaded region is where matter density is above $1.8\times 10^{-3} M_\odot$ pc^{-3} and correspond to the clustering of 2eV neutrinos. *Inset:* The surface density of the gas in the bullet cluster predicted by our collisionless matter subtraction method for the standard μ-function. The contour levels are [30, 50, 80, 100, 200, 300]$M_\odot pc^{-2}$. The origin in RA and dec is [$06^h 58^m 24.38^s$,-55°56'.32]

Testing GR with WL and galaxy clustering

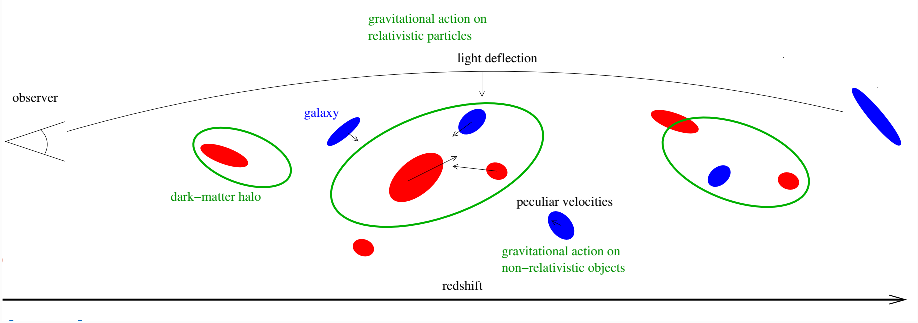

Results from SDSS

SDSS (Reyes et al. 2010)

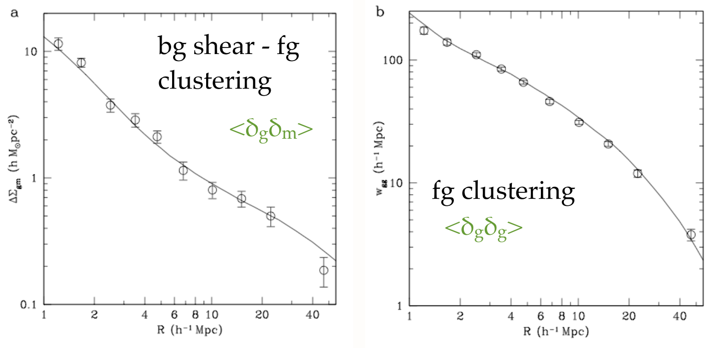

$$E_{\rm G} \cong \frac{1}{\beta} \frac{\langle \delta_{\rm m} \delta_{\rm g} \rangle}{\langle \delta_{\rm g} \delta_{\rm g} \rangle}$$

galaxy bias — growth factor

$$\beta = \frac{1}{b} \frac{{\rm d} \ln D_+}{{\rm d} \ln a}$$

$\beta = 0.309 \pm 0.035$

from SDSS galaxy clustering (redshift-space distortions) Tegmark et al. (2006)

Results from SDSS

Friedmann-Lemaître-Robertson-Walker metric with perturbations:

$$ds^2 = -(1 + 2\varphi)dt^2 + (1 - 2\phi)a^2 dx^2$$

time dilation spatial curvature

(Reyes et al. 201

- Galaxy-galaxy lensing: measures $\phi + \varphi$ and b
- Galaxy clustering: measures φ

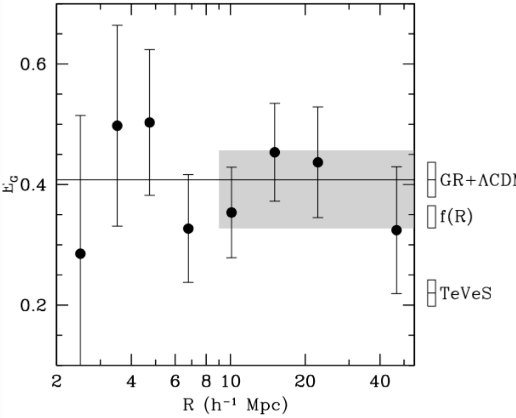

CMB (SZ) × WL

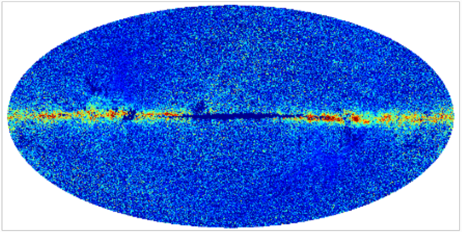

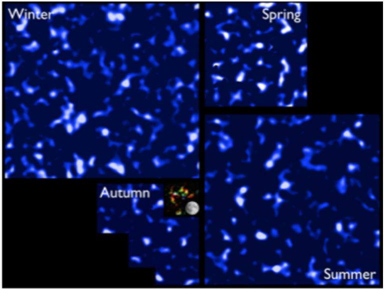

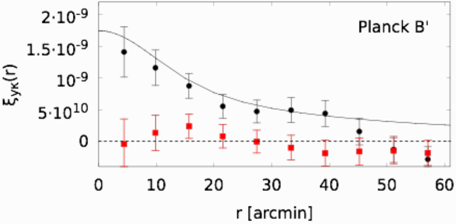

$$\left(\frac{b_{\rm gas}}{1}\right)\left(\frac{T_e(0)}{0.1\ \rm keV}\right)\left(\frac{\bar{n}_e}{1\ \rm m^{-3}}\right) = 2.01 \pm 0.31 \pm 0.21$$

(van Waerbeke et al. 2013b)

Planck CMB (SZ) × CFHTLenS weak-lensing: hot gas associated with matter

CMB lensing

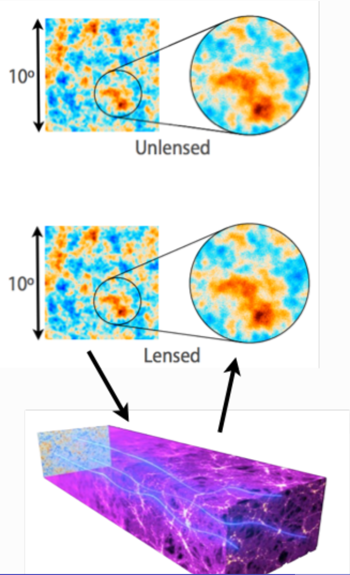
10°
Unlensed
10°
Lensed

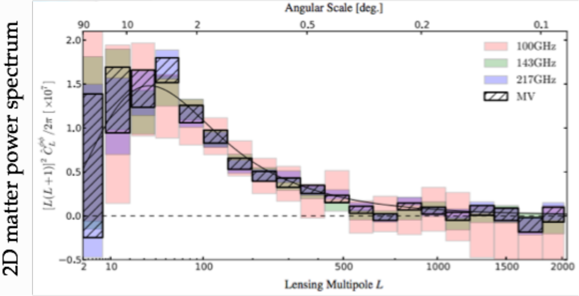
2D matter power spectrum
Angular Scale [deg.]
90
10
2
0.5
0.2
0.1
100GHz
143GHz
217GHz
MV
Lensing Multipole L
2
10
100
500
1000
1500
2000
2.0
1.5
1.0
0.5
0.0
−0.5

CMB lensing

Béthermin et al. (2013)
Planck Consortium (2014)
Holder et al. (2014)

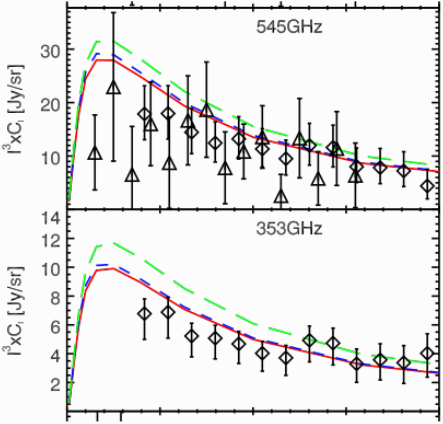

SPT CMB lens x Herschel CIB

Planck Consortium (2014)

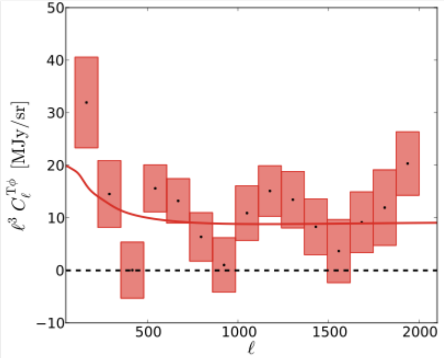

WL peak counts: Why do we want to study peaks?

- WL peaks probe high-density regions ↔ **non-Gaussian** tail of LSS
- **First-order** in observed shear: less sensitive to systematics, circular average!
- High-density regions ↔ **halo mass function**, but **indirect** probe:
  - Intrinsic ellipticity **shape noise**, creating false positives, up-scatter in S/N
  - **Projections** along line of sight

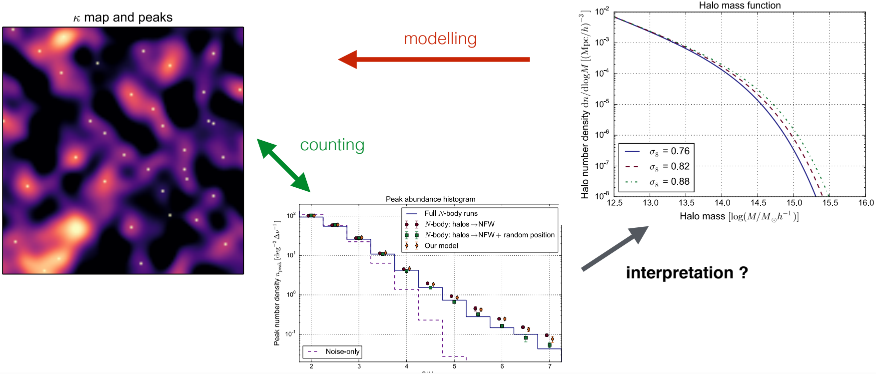

WL peak counts. What are peaks good for?

What do we gain from peak counting?

- Additional and complementary information and constraints compared to 2nd order shear
- Non-Gaussian information

Figure from Dietrich & Hartlap 2010

red/orange: cosmic shear

green: shear & peak

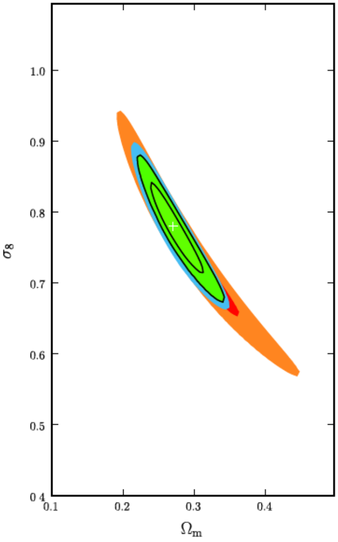

WL peaks: A fast stochastic model

Replace N-body simulations by Poisson distribution of halos

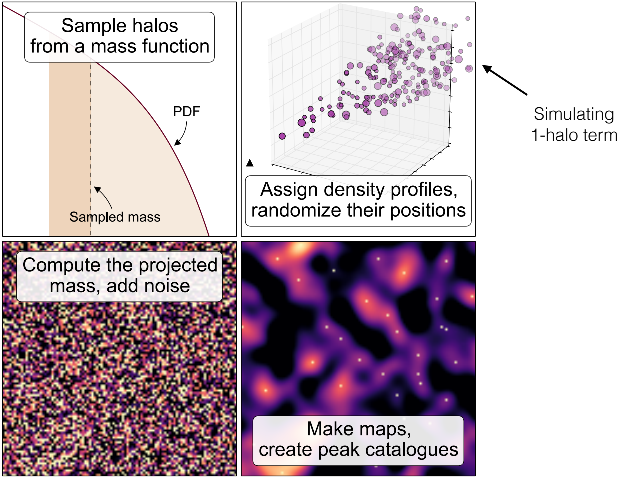

Lin, MK & Pires 2016

WL peaks: histograms

Hypotheses:

1. Clustering of halos not important for counting peaks (along los: Marian et al. 2013)
2. Unbound LSS does not contribute to WL peaks

Test:

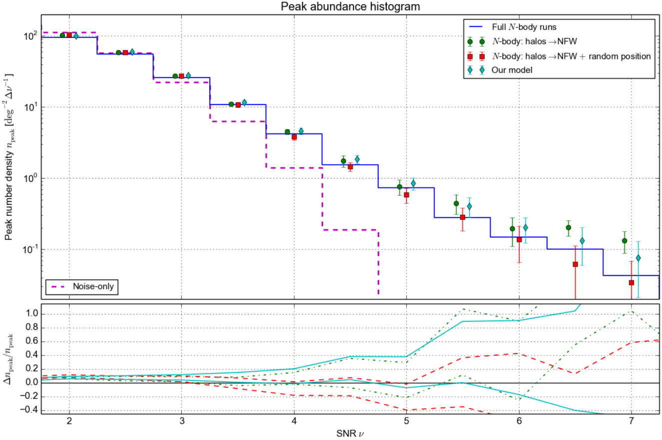

Field of view = 54 deg^2; 10 halo redshift bins from z = 0 to 1; galaxies on regular grid, z_s = 1.0

WL peaks: cosmological parameters

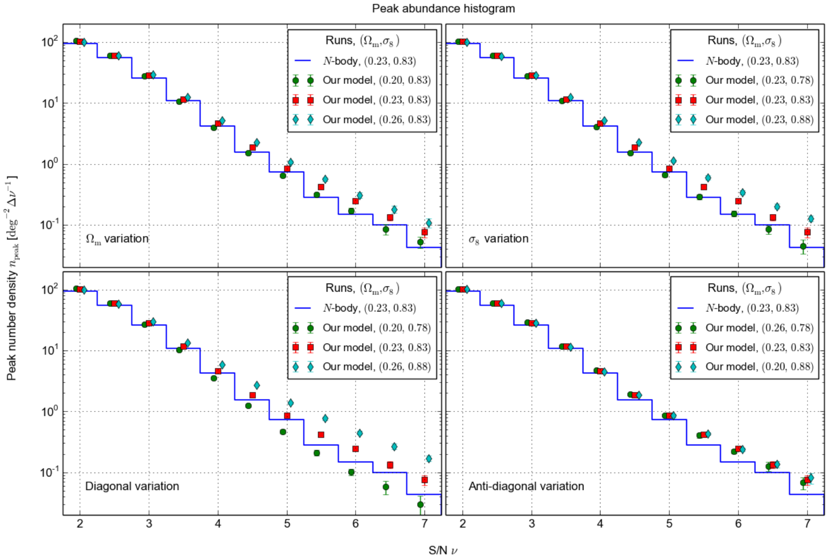

Lin & Kilbinger (2015a)

In general: Constraining cosmological parameters

Bayes' theorem

Likelihood: probability of data given parameters and model

Prior

$$p(\boldsymbol{\pi}|\boldsymbol{x}, m) = \frac{L(\boldsymbol{x}|\boldsymbol{\pi}, m)P(\boldsymbol{\pi}|m)}{E(\boldsymbol{x}|m)}$$

Posterior: probability of parameters given data and model

Evidence

$\boldsymbol{\pi}$: parameters
$\boldsymbol{x}$: data
m : *model*

Parameter constraints = integrals over the posterior

$$\int \mathrm{d}^n\pi \, h(\boldsymbol{\pi}) p(\boldsymbol{\pi}|\boldsymbol{x}, m)$$

For example:

$h(\boldsymbol{\pi}) = \boldsymbol{\pi}$: mean
$h(\boldsymbol{\pi}) = 1_{68\%}$: 68% credible region

Approaches: Sampling (Monte-Carlo integration), Fisher-matrix approximation, frequentist evaluation, ABC, …

WL peaks: data vector choices

Replace N-body simulations by Poisson distribution of halos

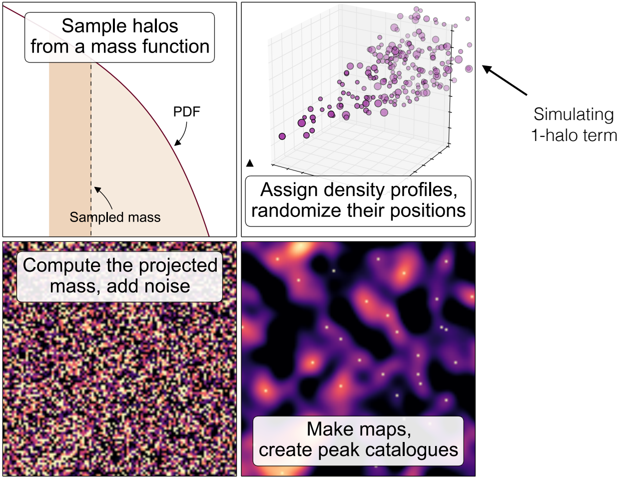

Lin, MK & Pires 2016

WL peaks: Gaussian likelihood

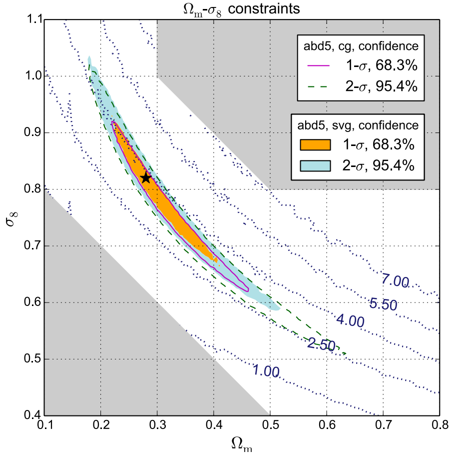

$$L_{\rm cg} \equiv \Delta \boldsymbol{x}^T(\boldsymbol{\pi})\, \widehat{\boldsymbol{C}^{-1}}(\boldsymbol{\pi}^{\rm obs})\, \Delta \boldsymbol{x}(\boldsymbol{\pi}),$$

$$L_{\rm svg} \equiv \Delta \boldsymbol{x}^T(\boldsymbol{\pi})\, \widehat{\boldsymbol{C}^{-1}}(\boldsymbol{\pi})\, \Delta \boldsymbol{x}(\boldsymbol{\pi}), \quad \text{and}$$

$$L_{\rm vg} \equiv \ln\left[\det \widehat{\boldsymbol{C}}(\boldsymbol{\pi})\right] + \Delta \boldsymbol{x}^T(\boldsymbol{\pi})\, \widehat{\boldsymbol{C}^{-1}}(\boldsymbol{\pi})\, \Delta \boldsymbol{x}(\boldsymbol{\pi}).$$

Cosmology-dependent covariance [(s)vg] reduces error area by 20%.

ABC: Approximate Bayesian Computation I

Likelihood:
probability of data given
parameters and model

$$p(\boldsymbol{\pi}|\boldsymbol{x}, m) = \frac{L(\boldsymbol{x}|\boldsymbol{\pi}, m) P(\boldsymbol{\pi}|m)}{E(\boldsymbol{x}|m)}$$

$\boldsymbol{\pi}$: parameters
$\boldsymbol{x}$: data
m : *model*

Likelihood: how likely is it that model prediction $\boldsymbol{x}^{\text{mod}}(\boldsymbol{\pi})$ reproduces data $\boldsymbol{x}$?

Classical answer: evaluate function L at $\boldsymbol{x}$.

Alternative: compute fraction of models that are equal to the data $\boldsymbol{x}$.

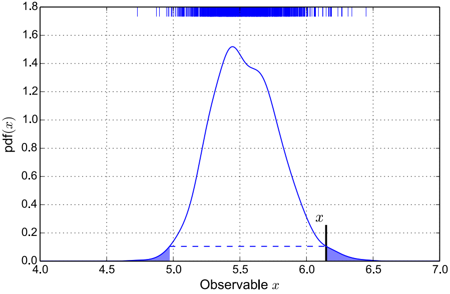

ABC: Approximate Bayesian Computation II

Probability = p/N in frequentist sense.

Magic: Don't need to sample N models. **One** per parameter π is sufficient with accept-reject algorithm.

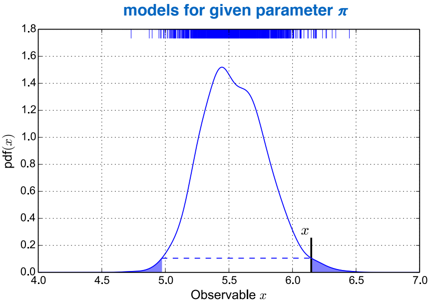

ABC can be performed if:

- it is possible and easy to sample from L

ABC is useful when:

- functional form of L is unknown
- evaluation of L is expensive
- model is intrinsically stochastic

ABC: Approximate Bayesian Computation III

Example: let's make soup.

Goal: Determine ingredients from final result.
Model physical processes? Complicated.

ABC: Approximate Bayesian Computation IV

Example: let's make soup.

Goal: Determine ingredients from final result.
Model physical processes? Complicated.
Easier: Make lots of soups with different ingredients, compare.

ABC: Approximate Bayesian Computation V

Example: let's make soup.

Questions:

- What aspect of data and simulations do we compare? (**summary statistic**)
- How do we compare? (**metric, distance**)
- When do we accept? (**tolerance**)

ABC: Approximate Bayesian Computation VI

Parameter constraints: ABC

- Summary statistic

  $\boldsymbol{s} = \boldsymbol{x}$ (data vector for 2 cases)

- Metric D: two cases

$$D_1\left(\boldsymbol{x}, \boldsymbol{x}^{\rm obs}\right) \equiv \sqrt{\sum_i \frac{\left(x_i - x_i^{\rm obs}\right)^2}{C_{ii}}},$$

$$D_2\left(\boldsymbol{x}, \boldsymbol{x}^{\rm obs}\right) \equiv \sqrt{\left(\boldsymbol{x} - \boldsymbol{x}^{\rm obs}\right)^T \boldsymbol{C}^{-1} \left(\boldsymbol{x} - \boldsymbol{x}^{\rm obs}\right)},$$

  D_1 in Lin & MK 2015b

  $D_1 + D_2$ in Lin, MK & Pires 2016

- ABC algorithm: iterative importance sampling (PMC) with decreasing tolerance

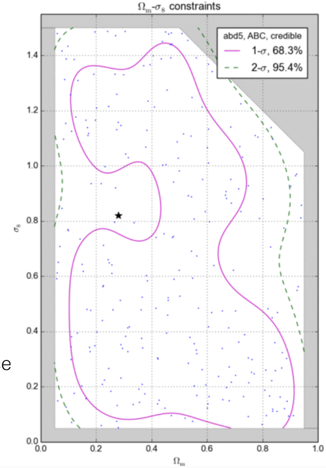

ABC: Approximate Bayesian Computation VII

ABC's accept-reject process is actually a sampling under P_ϵ (green curve):

$$P_\epsilon(\pi|x^{\rm obs}) = A_\epsilon(\pi) P(\pi),$$

where $P(\pi)$ stands for the prior (blue curve) and

$$A_\epsilon(\pi) \equiv \int {\rm d}x \; P(x|\pi) \mathbb{1}_{|x - x^{\rm obs}| \le \epsilon}(x),$$

is the accept probability under π (red area). One can see that

$$\lim_{\epsilon \to 0} A_\epsilon(\pi_0)/\epsilon = P(x^{\rm obs}|\pi_0) = \mathcal{L}(\pi_0),$$

so P_ϵ is proportional to the true posterior when $\epsilon \to 0$.

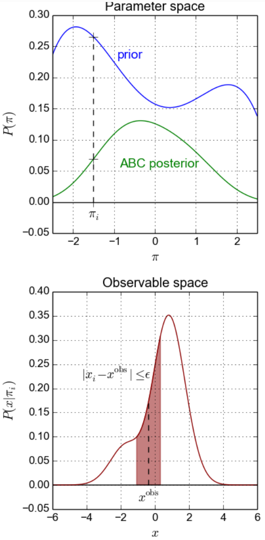

ABC: Approximate Bayesian Computation VIII

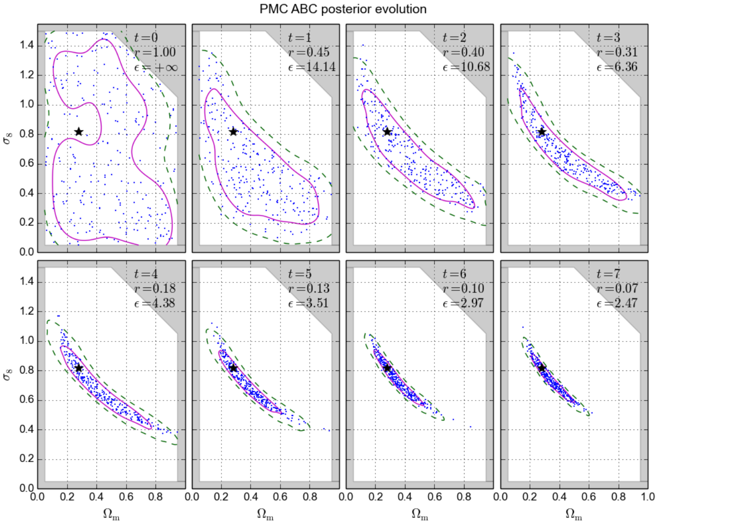

Lin & Kilbinger (2015b)

ABC: Approximate Bayesian Computation IX

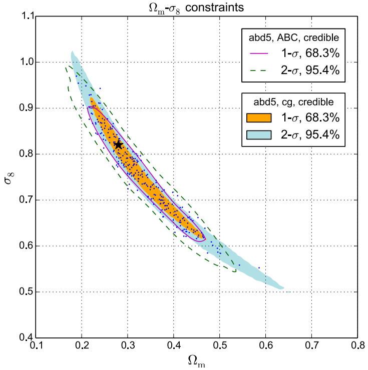

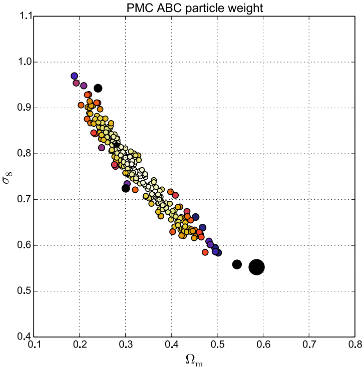

ABC wider but less elongated and less bent contours than Gaussian with const cov.
KDE smoothing effect?

Bibliography I

Bekenstein J D 2004 *Phys. Rev. D* **70**(8), 083509.

Benítez N 2000 *ApJ* **536**, 571–583.

Bernstein G M & Armstrong R 2014 *MNRAS* **438**, 1880–1893.

Bolzonella M, Miralles J M & Pelló R 2000 *A&A* **363**, 476–492.

Bonamente M, Hasler N, Bulbul E, Carlstrom J E, Culverhouse T L & al. 2012 *New Journal of Physics* **14**(2), 025010.
URL: *http://stacks.iop.org/1367-2630/14/i=2/a=025010*

Bradač M, Clowe D, Gonzalez A H, Marshall P, Forman W & al. 2006 *ApJ* **652**, 937–947.

Clowe D, Bradač M, Gonzalez A H, Markevitch M, Randall S W & al. 2006 *ApJ* **648**, L109–L113.

Codis S, Gavazzi R, Dubois Y, Pichon C, Benabed K & al. 2015 *MNRAS* **448**, 3391–3404.

Collister A A & Lahav O 2004 *PASP* **116**, 345–351.

Bibliography II

Fenech Conti I, Herbonnet R, Hoekstra H, Merten J, Miller L & al. 2017 *ArXiv e-prints* .

Gentile M, Courbin F & Meylan G 2012 *arXiv:1211.4847* .

Gentile M, Courbin F & Meylan G 2013 *A&A* **549**, A1.

Heymans C, Grocutt E, Heavens A, Kilbinger M, Kitching T D & al. 2013 *MNRAS* **432**, 2433–2453.

Heymans C, Van Waerbeke L, Miller L, Erben T, Hildebrandt H & al. 2012 *MNRAS* **427**, 146–166.

Hildebrandt H, Viola M, Heymans C, Joudaki S, Kuijken K & al. 2017 *MNRAS* **465**, 1454–1498.

Hirata C M, Mandelbaum R, Ishak M, Seljak U, Nichol R & al. 2007 *MNRAS* **381**, 1197–1218.

Hirata C M & Seljak U 2004 *Phys. Rev. D* **70**(6), 063526–+.

Huterer D, Takada M, Bernstein G & Jain B 2006 *MNRAS* **366**, 101–114.

Bibliography III

Ilbert O, Arnouts S, McCracken H J, Bolzonella M, Bertin E & al. 2006 *A&A* **457**, 841–856.

Jarvis M, Sheldon E, Zuntz J, Kacprzak T, Bridle S L & al. 2016 *MNRAS* **460**, 2245–2281.

Joachimi B, Cacciato M, Kitching T D, Leonard A, Mandelbaum R & al. 2015 *Space Sci. Rev.* **193**, 1–65.

Kaiser N, Squires G & Broadhurst T 1995 *ApJ* **449**, 460.

Kilbinger M, Fu L, Heymans C, Simpson F, Benjamin J & al. 2013 *MNRAS* **430**, 2200–2220.

Kuijken K 1999 *A&A* **352**, 355–362.

Kuijken K 2006 *A&A* **456**, 827–838.

Lima M, Cunha C E, Oyaizu H, Frieman J, Lin H & al. 2008 *MNRAS* **390**, 118–130.

Massey R & Refregier A 2005 *MNRAS* **363**, 197–210.

Melchior P, Viola M, Schäfer B M & Bartelmann M 2011 *MNRAS* **412**, 1552–1558.

Milgrom M 1983 *Astrophysical Journal* **270**, 371–389.

Bibliography IV

Miller L, Heymans C, Kitching T D, van Waerbeke L, Erben T & al. 2013 *MNRAS* **429**, 2858–2880.

Miller L, Kitching T D, Heymans C, Heavens A F & van Waerbeke L 2007 *MNRAS* **382**, 315–324.

Okura Y & Futamase T 2009 *ApJ* **699**, 143–149.

Planck Collaboration, Ade P A R, Aghanim N, Armitage-Caplan C, Arnaud M & al. 2014 *A&A* **571**, A17.

Refregier A 2003 *MNRAS* **338**, 35–47.

Reyes R, Mandelbaum R, Seljak U, Baldauf T, Gunn J E & al. 2010 *Nature* **464**, 256–258.

Schneider M D, Hogg D W, Marshall P J, Dawson W A, Meyers J & al. 2014 *ArXiv e-prints* .

Semboloni E, Hoekstra H, Schaye J, van Daalen M P & McCarthy I G 2011 *MNRAS* **417**, 2020–2035.

Simpson F, Heymans C, Parkinson D, Blake C, Kilbinger M & al. 2013 *MNRAS* **429**, 2249–2263.

Bibliography V

Singh S & Mandelbaum R 2016 *MNRAS* **457**, 2301–2317.

Tewes M, Cantale N, Courbin F, Kitching T & Meylan G 2012 *A&A* **544**, A8.

The Dark Energy Survey Collaboration, Abbott T, Abdalla F B, Allam S, Amara A & al. 2016 *Phys. Rev. D* **94**, 022001.

Van Waerbeke L, Mellier Y, Erben T, Cuillandre J C, Bernardeau F & al. 2000 *A&A* **358**, 30–44.

Velander M, van Uitert E, Hoekstra H, Coupon J, Erben T & al. 2014 *MNRAS* **437**, 2111–2136.

von der Linden A, Allen M T, Applegate D E, Kelly P L, Allen S W & al. 2014 *MNRAS* **439**, 2–27.

Walsh D, Carswell R F & Weymann R J 1979 *Nature* **279**, 381–384.

Zuntz J, Kacprzak T, Voigt L, Hirsch M, Rowe B & al. 2013 *MNRAS* **434**, 1604–1618.